

Dynamic Radius Jet Clustering Algorithm

Biswarup Mukhopadhyaya^a, Tousik Samui^a, and Ritesh K. Singh^a

^a*Department of Physical Sciences, Indian Institute of Science Education and Research Kolkata, Mohanpur, 741246, India.*

E-mail: biswarup@iiserkol.ac.in, tousiksamui@gmail.com,
ritesh.singh@iiserkol.ac.in

ABSTRACT: The study of standard QCD jets produced along with fat jets, which may appear as a result of the decay of a heavy particle, has become an essential part of collider studies. Current jet clustering algorithms, which use a fixed radius parameter for the formation of jets from the hadrons of an event, may be inadequate to capture the differing radius features. In this work, we develop an alternative jet clustering algorithm that allows the radius to vary dynamically based on local kinematics and distribution in the η - ϕ plane inside each evolving jet. We present the usefulness of this dynamic radius clustering algorithm through two Standard Model processes, and thereafter illustrate it for a scenario beyond the Standard Model at the 13 TeV LHC.

Contents

1	Introduction	1
2	Methodology	3
2.1	Standard Sequential Recombination Algorithms	3
2.2	Our Proposal: Dynamic Radius Jet Clustering Algorithm	4
3	Application to Standard Model Processes	7
3.1	Illustration I: $pp \rightarrow tj$ process	8
3.2	Illustration II: $pp \rightarrow Vj$ Subprocess	15
4	Usefulness in BSM signals	19
5	Summary and Outlook	25

1 Introduction

The physics extraction capacity of any high-energy collider depends crucially on the handling of coloured particles in various final states. These are produced as partons via either short-distance interactions of quantum chromodynamics (QCD) or electroweak processes [1, 2]. The partons, however, hadronize through long-distance QCD effects which are not calculable *ab initio*. One rather uses semi-empirical methods to predict the probability that energetic partons will fragment into more low-energy partons and ultimately form colour-neutral hadrons which are observable in the detector. Groups of closely spaced hadrons with varied degrees of collimation form ‘jets’ whose identification, isolation, and merger are predicted once more with the help of semi-empirical (and by no means uniquely decided) algorithms called jet clustering algorithms [3–7]. The aim always remains to define jets with such algorithms which most accurately elicit the short-distance physics underlying the events that are studied. They thus constitute some of our most important tools in the analysis of phenomena at colliders.

In the context of the Large Hadron Collider (LHC), a widely used class of jet criteria is based on so-called k_t -type sequential recombination jet algorithms [7–13]. These algorithms (briefly discussed in the next section) typically try to merge ‘neighbouring’ hadrons to identify the group as a jet. The neighbourhood of a hadron is defined by a single radius parameter R_0 in the η - ϕ plane of the detector, which is used to quantify the radius (or size) of a jet. This is because the hadrons within R_0 are merged to form a jet while the hadrons outside R_0 are not included in that jet. The choices for the value of R_0 in these algorithms depend on the physics searches one is carrying out. At the 13 TeV LHC, the typical choices for R_0 are 0.4 or 0.8 for a ‘narrow’ or a ‘fat’ jet, respectively. There are, in addition, jet isolation criteria depending on whether one is trying to separate a jet from a hard lepton or another hadronic jet. However, the sequential recombination algorithms generally do not accommodate varying choices of radii on a jet-by-jet basis in a single event since they

have a single constant parameter that determines the radius of a jet. Separate classifiers for a ‘narrow’ jet and a ‘fat’ jet in a single event in the current k_t -type algorithms are thus difficult to set. An important improvement over the current fixed radius algorithms would be to make them adapt the jet radii dynamically jet-by-jet in each event. We make an attempt in this direction in this work.

Our central idea of choosing the radius dynamically of a jet, especially for a boosted fat jet, is based on the kinematics of the decay products of the initiating heavy particle. From the theoretical side, the formation of boosted fat jet occurs due to the high collimation of the on-shell decay products – and their showering and subsequent hadronization – of the energetic and therefore boosted heavy particles. This is very different from the formation of light quark- or gluon-initiated jets, whose collimation is primarily due to parton showering and subsequent hadronization. On the other hand, at the operational level, as per the standard k_t -type algorithms, the fat jets are formed in the same way as the regular ‘narrow’ jets, which are initiated by light quarks or gluons. However, the kinematics of on-shell decay products and their radiation pattern of a heavy particle is different from the showering of energetic light quarks or gluons. Therefore, the internal structure of a fat jet is very different from a narrow one. This internal structure has been used to tag different heavy and light jets in the LHC context. For example, jet substructure (JSS) observable generalized angularities λ_β^κ [14, 15] is used to distinguish between quark- and gluon-initiated jets [16–26]. The same variable was used in the classification among the narrow jet, fat W jet, or boosted top jet [27–30]. Another important set of JSS observables, namely the energy correlation functions (ECFs) [31, 32], was shown to be useful in classifying different types of jets [29, 33–37]. The observable N -subjettiness (τ_N) [38, 39] has been used to find the multi-pronged nature of light or heavy jets [40–65]. These variables have also been used extensively by the experimental collaborations at the 13 TeV LHC [66–68]. These examples try to exploit the energy distribution pattern inside a jet to distinguish a heavy object from a QCD jet. The common theme of these jet substructure variables is the utilization of the ‘multi-pronged’ nature of the fat jets. Due to this multi-pronged nature, one expects the variance of inter-constituent distance ΔR of a fat jet to be significantly different compared to the narrow QCD jets. This variance of a jet can be used to grow the radius of a jet starting from an initial radius. Earlier attempts to make the jet radius variable, albeit with somewhat different motivations and formalisms, can be found in references [69, 70]. In Ref. [69], the effective radius of a pseudojet during their evolution was taken to be inversely proportional to the p_T with a maximum cut-off on the radius. Essentially, this algorithm starts from a big effective radius and the size shrinks as a process of evolution. On the other hand, in Ref. [70], an expectation-maximization approach was taken for clustering the hadrons into a pre-determined number of clusters (jets). Our approach, in this work, is to modify the standard fixed radius k_t -type algorithms to make the radius grow depending on the local kinematics and distribution (in the η - ϕ plane) of the hadrons.

The rest of the article is organized as follows. In section 2, we briefly outline the k_t -type sequential recombination algorithms followed by our improvement to the same. We test the efficacy of our algorithms on two SM processes and discuss them in section 3. Section 4 deals with one application in the BSM scenario. We summarize and conclude in section 5.

2 Methodology

2.1 Standard Sequential Recombination Algorithms

At the operational level, a jet is constituted by a bunch of four-momenta obtained using some clustering algorithm. Among various possible ways of grouping up the four-momenta of an event, we need to choose those relevant to physics at the collider. It is important that the clustering algorithm should ensure infrared and collinear (IRC) safety, which, in our context, can be defined in terms of the following conditions [7]:

Infrared (IR) safety: The output of the algorithm should not be affected by the introduction of a four-momentum with $p \rightarrow 0$.

Collinear (C) safety: The output of the algorithm should not be affected by a collinear splitting of any four-momentum.

The algorithm that best takes care of the issue of IRC safety is known as k_t -type sequential recombination jet clustering algorithms [7]. We briefly outline these algorithms below¹.

If an event consists of N final state particles, whose four-momenta are taken in a list as an input of the k_t -type algorithms. The distance d_{ij} between the i^{th} and j^{th} four-momenta and the distance d_{iB} between the i^{th} and the beam are then defined as

$$d_{ij} = \min \left(p_{T_i}^{2p}, p_{T_j}^{2p} \right) \Delta R_{ij}^2, \quad (2.1)$$

$$d_{iB} = p_{T_i}^{2p} R_0^2, \quad (2.2)$$

where R_0 is the radius parameter of the algorithm, ΔR_{ij} is the Euclidean distance between the i^{th} and j^{th} four-momenta in the η - ϕ plane, and p_{T_i} is p_T of i^{th} four-momenta. The exponent p sets the weight factor to the Euclidean distance in the η - ϕ plane. The three choices of $p = 1, 0$ and -1 correspond to the k_t (KT) [8–10], Cambridge-Aachen (CA) [11, 12], and anti- k_t (AK) [13] algorithms, respectively. The algorithm for combining nearby four-momenta with respect to the above distance measures to form jets has the following steps.

Step 1. The distances d_{ij} for all the possible pairs and beam distances d_{iB} for all the four-momenta are calculated first.

Step 2. The minimum among all the d_{ij} and d_{iB} 's is determined.

Step 3a. If the minimum occurs at one of the i, j pairs, the corresponding i^{th} and j^{th} four-momenta are merged to form a new four-momentum. The older ones, i^{th} and j^{th} four-momenta are removed from the list and the newly merged one is added to the list and goes back to Step 1.

Step 3b. On the other hand, if the minimum distance is one of the d_{iB} , the i^{th} four-momenta is declared as a final jet, and it is removed from the list and goes back to Step 1.

¹Here, we only discuss the inclusive algorithms in the LHC context. For other jet clustering algorithms, please see Ref. [7].

Step 4. The process is stopped once the list gets empty.

This class of algorithms is seedless because the clustering of four-momenta to form a jet does not start from a particular seed. Rather, the algorithms try to merge the closest pair first. A group of hadrons is then declared as a jet when an appropriate size is reached. The essential difference among the three different algorithms, *viz.* AK, CA, and KT is that they give different weights to the Euclidean distance in the η - ϕ plane. This typically sets some sort of seed to the clustering algorithms in the sense that it gives a preference to a hadron around which four-momenta merge to give rise to a final jet. In the case of the KT algorithm, it is the softer (in terms of p_T) constituent which merges first and then the harder ones get attached to it. As a result, the shape of the final jet may not be circular in the η - ϕ plane. On the other hand, in the AK algorithm, the hardest particle in a neighbourhood becomes some sort of seed for the jet and the softer ones merge at a later stage. Hence the final jet looks circular in the η - ϕ plane. In the CA algorithm, the merging is purely angular. Among the three algorithms, the AK algorithm is the most popular one owing to its circular shape. Importantly, in the k_t -type algorithms, there is a fixed radius parameter R_0 , whose value dictates the typical size of all the jets in a particular event. We note that these algorithms are unable to capture the essential features of the events where narrow and fat jets may simultaneously arise. In our proposed algorithm, we have modified these algorithms to bring out the features of varying sizes of the jets.

2.2 Our Proposal: Dynamic Radius Jet Clustering Algorithm

The usual k_t -type algorithms take a fixed radius as an input parameter, and hence the algorithms return all the jets to be of the same size (or narrower) in a single event. This lack of dynamicity in choosing a radius can be overcome by setting the radius parameter dynamically during the construction of each jet.

In any k_t -type algorithm, the starting point is a list of N four-momenta of particles. We will refer to these as fundamental particles or, sometimes, fundamental four-momenta. The algorithm follows Steps 1 to 3b, as defined in section 2.1, iteratively until the list gets empty. At every iteration, the number of contents of the list gets reduced by one. The reduction happens in two ways: (1) via the merger of two four-momenta, (2) via the declaration of four-momentum as a final jet. Thus at an intermediate iteration, the list contains two different types of objects. These two types of objects are (1) fundamental four-momenta, and (2) composite four-momenta, generated through the merger of two or more fundamental four-momenta. These composite objects evolve through iterations to give rise to the final jets. For our convenience, let us label these composite evolving objects as pseudojets. We borrowed the name pseudojet from the `PseudoJet` class in the `FastJet3` package [71], where all the types of four-momenta are called pseudojet. However, we will call them by different names: fundamental, pseudojet (composite or evolving), and jet (or final jet).

Our proposal is to change the constant nature of the radius parameter R_0 in Eq. (2.2) to a dynamic quantity depending on the distribution, in the η - ϕ plane, of the fundamental objects inside each evolving pseudojet. Therefore, the modified distance measure for the

dynamic radius algorithm takes the form

$$d_{ij} = \min \left(p_{T_i}^{2p}, p_{T_j}^{2p} \right) \Delta R_{ij}^2, \quad (2.3)$$

$$d_{iB} = p_{T_i}^{2p} R_{d_i}^2, \quad (2.4)$$

where R_{d_i} is the dynamical radius parameter, defined as

$$R_{d_i} = R_0 + \sigma_i. \quad (2.5)$$

The constant R_0 is an input parameter similar to the standard k_t -type algorithm and it is the starting point of the dynamical growth of the radius of an evolving jet. For the i^{th} pseudojet, σ_i is calculated as

$$\sigma_i^2 = \frac{\sum_{a < b} p_{T_a} p_{T_b} \Delta R_{ab}^2}{\sum_{a < b} p_{T_a} p_{T_b}} - \left(\frac{\sum_{a < b} p_{T_a} p_{T_b} \Delta R_{ab}}{\sum_{a < b} p_{T_a} p_{T_b}} \right)^2, \quad (2.6)$$

where the summation indices a and b run over the fundamental constituents of the pseudojet. The modifier σ_i of the radius parameter in Eq. (2.6) is basically ‘ p_T -weighted’ standard deviation of the distances between pairs of fundamental constituents of an evolving pseudojet. In our proposal, this standard deviation σ_i is used to capture the size feature of an evolving jet dynamically. For a single fundamental four-momentum, σ_i is taken to be zero.

The motivation for choosing the modifier of the radius parameter to be p_T -weighted standard deviation is as follows. As more than one fundamental objects merge to become a new pseudojet, it no longer represents a single point in the η - ϕ plane; it is a composite object whose constituents are distributed in that plane. The standard deviation σ_i for a pseudojet i , defined in Eq. (2.6), provides a measure of its fuzziness. We want to incorporate this fuzziness in the radius parameter. In the measure of its fuzziness, we also want the harder components to be more dominant than the softer ones. Essentially, if the pseudojet is dominated by a single p_T -hard fundamental constituent or many extremely collimated but similar p_T objects, we do not want its radius to get increased further. This is because, in these scenarios, the final jet is expected to be a narrow jet. On the other hand, if the pseudojet has more than one p_T -hard fundamental constituents slightly separated, we expect it to be a fat jet and therefore need an increment to its radius. Both of these two aspects are taken care of by the p_T -weighted standard deviation in Eq. (2.6).

Thus, in our proposal, we first take a starting radius R_0 to be our input parameter. The algorithm then calculates R_{d_i} for each pseudojet, which at an intermediate state accumulates some constituents. At every iteration, the value of the dynamic radius parameter is calculated as the sum of the starting radius R_0 and the radius modifier σ . In a nutshell, the proposed algorithm starts from an initial radius R_0 and grows its radius dynamically using the information from the distribution of its constituents in the $\eta - \phi$ plane.

In the proposed algorithm, the exponent p to the p_T in the expressions of distance measures d_{ij} and d_{iB} in Eqs. (2.3–2.4) can take three possible values. We will call the

corresponding algorithms as dynamic radius AK (DR-AK), dynamic radius CA (DR-CA), and dynamic radius KT (DR-KT) jet clustering algorithms.

The IRC safety of the algorithm through the definitions provided in section 2.1 can be approximately ensured in the radius modifier σ as well as in the final output of the algorithm. With the introduction of an additional four-momentum, say p_q , the additive contributions to the numerators and to the denominators of the two terms in Eq. (2.6) can be generically written as $p_{T_q} \sum_a (p_{T_a} \Delta R_{aq}^\alpha)$ (for the denominators, $\alpha = 0$, and for the two numerators $\alpha = 1$ and 2). Clearly, all the additive contributions go to zero as $p_{T_q} \rightarrow 0$, thereby ensuring the IR safety of the quantity σ_i for i^{th} pseudojet. For the consideration of IR safety of the algorithm, let us assume an extra particle of momentum p_q is introduced in an existing event. This extra particle actively participates in the clustering process only by one of the three actions: (a) by getting merged to another fundamental particle, (b) by getting recombined to a composite pseudojet, or (c) by getting declared as a singleton jet. The action (a) does not change the value of σ or the four-momentum of the pseudojet after the merger of the four-momentum with $p_q \rightarrow 0$. The same is true for the merger of p_q via action (b) since the merger of two fundamental four-momenta keeps the value of σ at zero. After the merger of this $p \rightarrow 0$ four-momentum, both the radius modifier σ and the total momentum remain unaffected. After this merger, the rest of the clustering process does not get affected, and hence the final output of the clustering algorithm remains unaffected. Furthermore, action (c) does not give rise to an extra jet whenever $p \rightarrow 0$.

For the collinear safety, one can see that the radius modifier σ remains almost unaltered when a four-momentum is split collinearly. Let a four-momentum p_q gets split into p_r and p_s . Any general term $p_{T_a} p_{T_q} \Delta R_{aq}^\alpha$ then becomes $p_{T_a} (p_{T_r} \Delta R_{ar}^\alpha + p_{T_s} \Delta R_{as}^\alpha)$. In the collinear splitting limit, $p_{T_q} = p_{T_r} + p_{T_s}$, $\Delta R_{ar} = \Delta R_{as} = \Delta R_{aq}$. Moreover, there will not be any additional contribution due to the p_r and p_s combination except for the denominators in Eq. (2.6) since $\Delta R_{rs} = 0$. This ensures an approximate collinear safety of σ_i for any i^{th} pseudojet. On the other hand, for the collinear safety of the algorithm, if any four-momentum collinearly splits into two four-momenta, then the distance $d_{ij} \rightarrow 0$. Hence, these two collinearly split four-momenta get merged together at a very early stage; a feature that is inherently present in the k_t -type algorithm. Other IRC safety features (due to p_T -dependent prefactors in the d_{ij} and d_{iB} definitions) of the standard k_t -type algorithms will be inherited by the dynamic radius algorithm.

We have implemented the method of dynamic radius jet clustering algorithm as a **FastJet3** plug-in [71, 72]. This package has many built-in data-types and functionalities to optimize the implementation and computation of jet clustering algorithms. In particular, we have used **NNBase** and **NNH** classes to help us keep track of the distance measures. As required by these two classes, our d_{ij} measure is also symmetric in i and j indices. The **ClusterSequence** class has then been used to merge two four-momenta and keep track of the clustering sequence. The **PseudoJet** class has been used to store the four-momenta information of all the initial, intermediate, and final jets. The **user_info** property of **PseudoJet** data-type has been used to store the information related to the radius modifier σ_i of the i^{th} pseudojet. This way of implementation has at most N^2 computational com-

plexity for an event of size N . The worst possible complexity arises when all the particles in an event are merged to form a single jet. Since this worst possibility does not generally occur, we expect the computational expense to be less in a practical scenario. We note that the standard k_t -type algorithms also have N^2 complexity via the basic implementation of the FastJet algorithm [71, 72].

One important point to note is that the equations for distance measures, defined in Eqs. (2.1–2.2), can be recast to in the radius parameter in the expression of d_{ij} rather than in the expression of d_{iB} . That is to say that the modified set of equations can be taken to be

$$\tilde{d}_{ij} = \min(p_{T_i}^{2p}, p_{T_j}^{2p}) \left(\frac{\Delta R_{ij}}{R_0} \right)^2 \quad (2.7)$$

$$\tilde{d}_{iB} = p_{T_i}^{2p} \quad (2.8)$$

The standard sequential recombination algorithm yields identical results in both formalisms since the radius is a constant parameter. However, if this latter formalism is chosen to incorporate dynamicity, the form of the dynamic radius parameter R_d will be different. The dynamic radius R_d , in this type of modification, will be dependent on both pseudojets. One option would be to add the standard deviations σ_i and σ_j of the i^{th} and j^{th} pseudojets, respectively, to the constant parameter R_0 . This way of defining R_d ensures the symmetry in i and j indices and, therefore, the implementation of the method via NNBase and NNH as a FastJet3 plug-in can easily be performed. In any case, the output of the algorithm is modified according to Eq. (2.7–2.8) will be different from that of the one considered in Eq. (2.3–2.4).

We now are ready to apply our formalism to some simple SM processes and check how it performs compared to the standard sequential recombination algorithms. We discuss this in the next section in connection with SM processes and consider its application to BSM in the section after that.

3 Application to Standard Model Processes

We take the following two SM processes to illustrate the performance of our newly developed algorithm.

I. $pp \rightarrow tj$

II. $pp \rightarrow Vj$, ($V = W$ or Z)

For both cases, we have generated parton-level events using MadGraph5 (MG5) [73]. We will refer to these events as MG5 parton-level events and the final state partons in these events as MG5 partons. A lower cut of 500 GeV on the p_T of the jets has been imposed during the generation of the MG5 parton-level events. This helps us in generating events with boosted top or vector bosons at the parton-level, which then form fat jets after subsequent decays and hadronization. For the purpose of the following studies, only the hadronic decays of top and W/Z are considered. We have then passed the MG5 parton-level events to

Pythia8 [74, 75] for showering and hadronization. The *Monash 2013 Tune* [76], the default tune of Pythia8, has been used to take care of the simulations of underlying events and multi-parton interactions in the proton-proton collisions. The output of Pythia8 has then been transferred to FastJet3 for the formation of jets.

3.1 Illustration I: $pp \rightarrow tj$ process

The top quark, when highly boosted, results in a fat jet while the j yields a narrow jet after the effects of showering and hadronization. In order to compare various jet properties between the dynamic radius and fixed radius algorithm, we run these two types of algorithms on the same set of hadrons from each event. We first demonstrate how the dynamic radius algorithms help in capturing the fat and narrow objects in a single event. This has been demonstrated by depicting the hadrons and jets of an example event in Fig. 1, where we plotted, in the η - ϕ plane, the position of the hadrons in the event along with the high- p_T jets constructed out of these hadrons. The sizes of the dots are kept proportional to $\sqrt{p_T}$ of the hadrons. The jets are represented by the unfilled black circles and the solid dots inside the black circles comprise of the constituent hadrons of the jets. The three panels on the left show the jets for (a) AK, (c) CA, and (e) KT jet algorithms with $R_0 = 0.5$. In all the left panels, the algorithms return three high- p_T jets; one near (2,2) position and the other two are near (0,5) position in the η - ϕ plane. With the MG5 parton-level information, we identified that the jet in (2,2) position is initiated by j while the two jets near the (0,5) position is initiated by the decay products of the hard top quark. Because of fixed radii of the standard k_t -type jet clustering algorithms, they could not capture all the hadrons initiated by the decay products of the top quark inside a single jet; rather they have been split into two different jets. A quick fix to this problem would be to increase the size of the radius parameter. This prescription, however, ends up increasing the jet size unnecessarily, for example at the (2,2) position where such increment is not required. This unnecessary increase in the radius of a jet increases jet mass, especially in the high pile-up scenario. One interesting option in such cases would be to choose the radius according to the need of a jet. This is precisely where the dynamic radius jet clustering algorithm is useful in this type of scenario. This can be seen in the three panels on the right in Fig. 1. There the hadrons and the high- p_T jets are drawn for dynamic radius jet clustering algorithms with $R_0 = 0.5$. The interesting point to note in all three right panels is that there are two jets instead of three. The radius of the jet near the (0,5) position has been appropriately grown to capture the full decay products of the top quark and their radiations while the radius of the jet near the (2,2) position did not grow much. This desirable characteristic of a jet algorithm would be beneficial for the studies of collider events, where narrow as well as fat jets are expected to occur simultaneously. In all the panels, the radius of each black circle is kept to be equal to the final radius R_d , as defined in Eq. (2.5), of each individual jet. For the fixed radius jet algorithms, the final radius is essentially the fixed radius parameter R_0 .

Fig. 1 gives an approximate idea of how the dynamic radius helps us in finding a fat jet starting from a small radius. Next, we show how often this dynamic radius jet algorithm helps us in finding the fat jet. In order to demonstrate that, we have employed the following

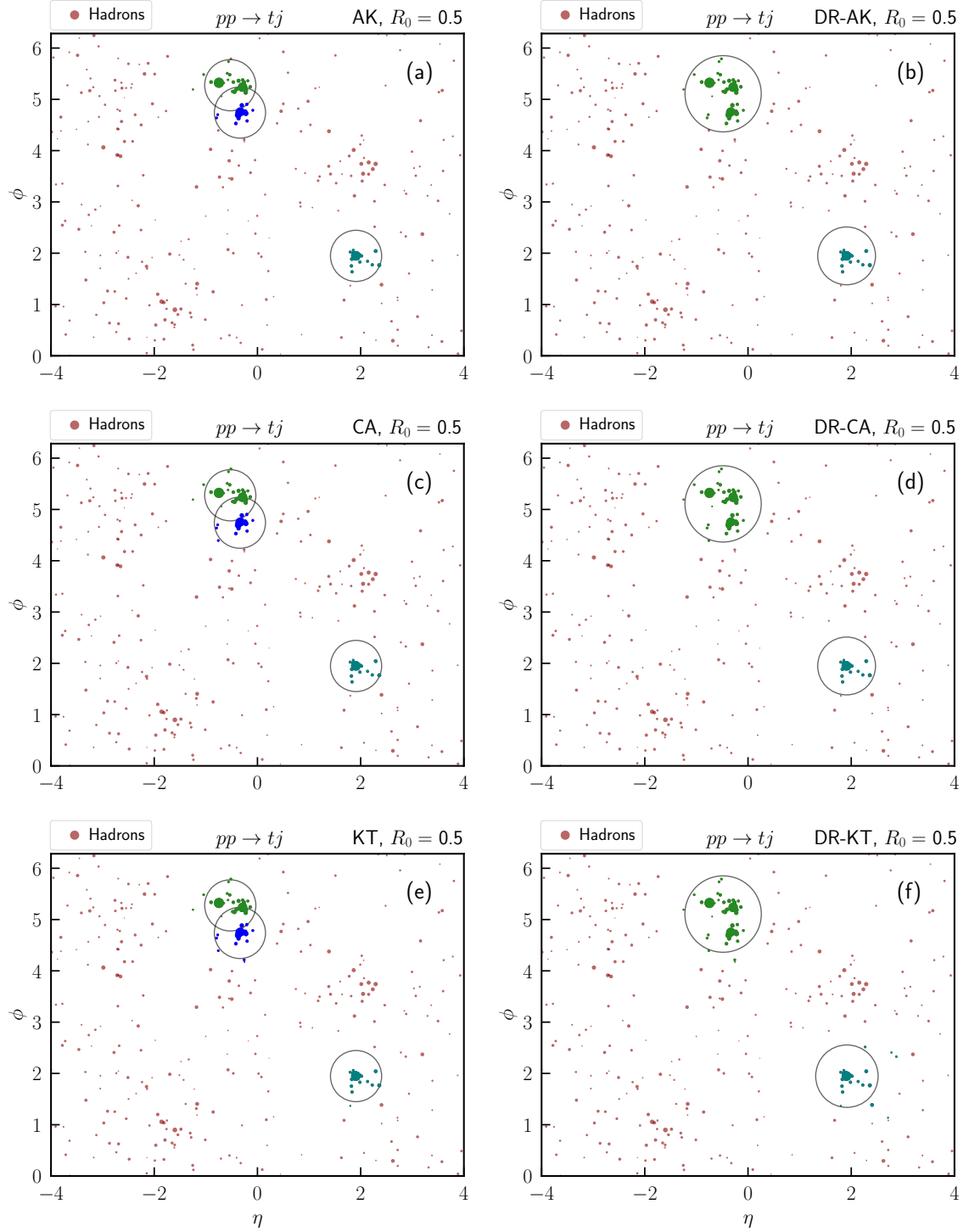


Figure 1: Positions of final state hadrons and jets in the η - ϕ plane in an example event for $pp \rightarrow tj$ process. The red dots represent the final state hadrons and their sizes are kept proportional to $\sqrt{p_T}$ of the corresponding hadron. The unfilled circles represent the final radius R_d of a jet. The teal coloured dots represent the constituents of the hard ‘narrow’ jets. The green and blue (wherever applicable) dots represent the constituents of the fat *top* jet. The left panel, from top to bottom, is for (a) AK, (c) CA, and (e) KT algorithms with $R_0 = 0.5$. The right panel, from top to bottom, represents jets clustered using (b) DR-AK, (d) DR-CA, and (f) DR-KT algorithms, respectively, with $R_0 = 0.5$.

procedure. We first form the jets from the hadrons and choose only the high- p_T (> 5 GeV) jets. We then tag the energetic jets, event by event, as reconstructed ‘top’ or reconstructed ‘jet’ with the help of MG5 parton-level information. The events are classified into two categories, as described below.

A1. Category A1 consists of events satisfying the following conditions.

- A jet should have mass in the range (150, 200) GeV and have $\Delta R(\text{top}^{\text{truth}}, \text{jet}) < 0.5$. This jet is identified as a reconstructed top jet. We label these reconstructed objects as ‘*top* (A1)’ in the subsequent discussions.
- After the tagging of the top jet, another jet should have $p_T > 300$ GeV and should be within 0.5 distance from the original jet as generated by MG5. These jets are labelled as ‘*jet* (A1)’ in further discussions.

A2. Category A2 are the events which satisfy the following conditions.

- Two separate jets within 1.0 distance of the original top quark and having an invariant mass between 150 and 200 GeV. These two jets are tagged as constituent jets of the reconstructed top jet, which is a combination of these two constituents. These combinations are labelled as ‘*top* (A2)’.
- Another jet having $p_T > 300$ GeV and within 0.5 radius from the original jet. This is labelled as ‘*jet* (A2)’.

In general, any inclusive kt -type clustering algorithm yields as output many soft jets along with the hard ones. The origin of these soft jets is primarily the soft radiation due to underlying events and wide angle parton shower. These jets are expected in both the category A1 and A2 events. Any jet having $p_T > 5$ GeV and labelled neither as *top* nor as *jet* is labelled as *soft jet*.

The two categories have been chosen to demonstrate the usefulness of the dynamic radius jet algorithm. Category A1 captures the whole *top* jet by the jet clustering algorithm while the events in category A2 need post-processing after the jet clustering. Therefore, a desirable criterion of a better-performing jet clustering algorithm would be to have more events in category A1. In order to illustrate that, for a given category, we define acceptance efficiency

$$\mathcal{A} = \frac{\text{number of events accepted in a particular category}}{\text{total number of events}}. \quad (3.1)$$

After the classification of the events into the above two categories, the distribution of distances between the MG5 parton-level objects and reconstructed ones are plotted in Fig. 2. In both the panels of the figure, the blue and brown histograms are for *top* jets, and the green and red ones are for energetic *jets*. The corresponding categories of the histograms are mentioned alongside the legends. The distributions are shown for jets clustered using the AK algorithm with (a) $R_0 = 0.5$, and (b) $R_0 = 0.8$. Since this distance between the MG5 parton-level and reconstructed ones are features of parton showering and hadronization, the normalized distributions are kind of identical for different radius

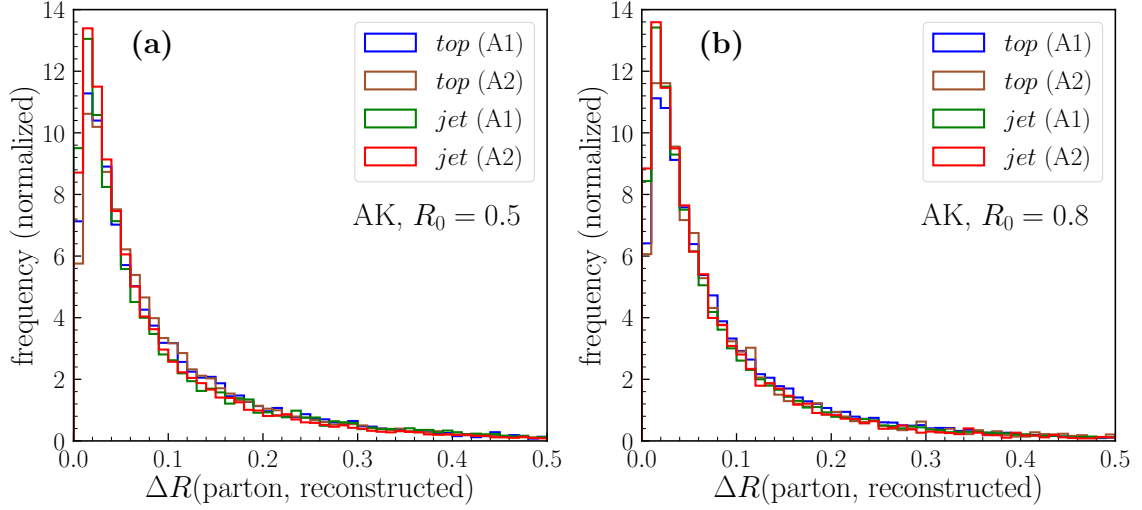


Figure 2: Normalized distribution of ΔR between the MG5 parton-level object and corresponding reconstructed jet. The jets were clustered using the AK algorithm with radius parameters (a) 0.5 and (b) 0.8.

choices. These ΔR distributions are very similar even with different choices of standard or dynamic radius sequential recombination algorithms and, therefore, are not shown to avoid repetition. This distribution also justified the choice of 0.5 radius to find reconstructed objects from the MG5 partons.

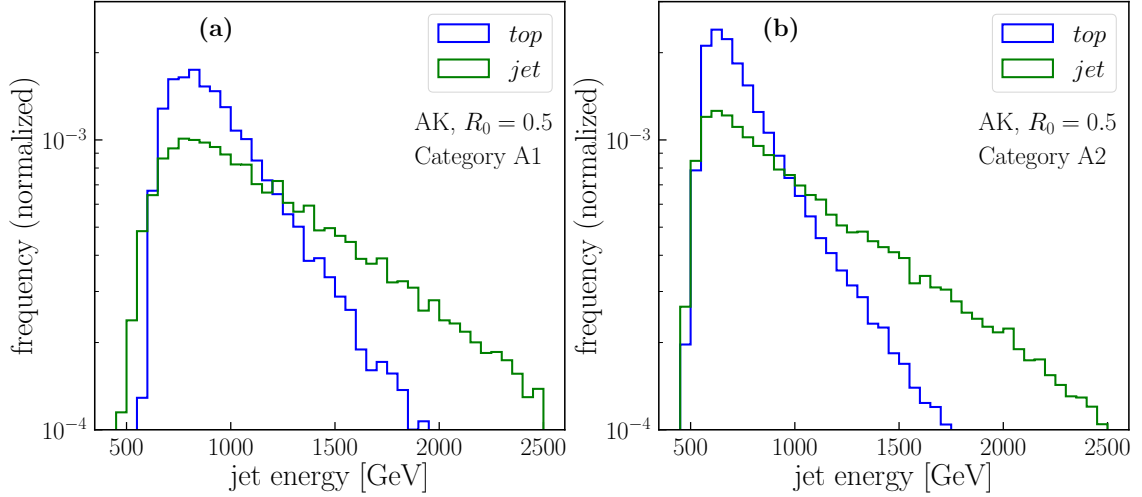


Figure 3: Normalized distribution of jet energy for categories (a) A1 and (b) A2. The blue and green histograms are respectively for the reconstructed *top* and the high- p_T *jet*.

We show in Fig. 3 the jet energy distributions for the objects of our study. The left and right panels show the distributions for categories A1 and A2, respectively. The blue and green histograms are for the *top* and the high- p_T *jet* produced in association with it.

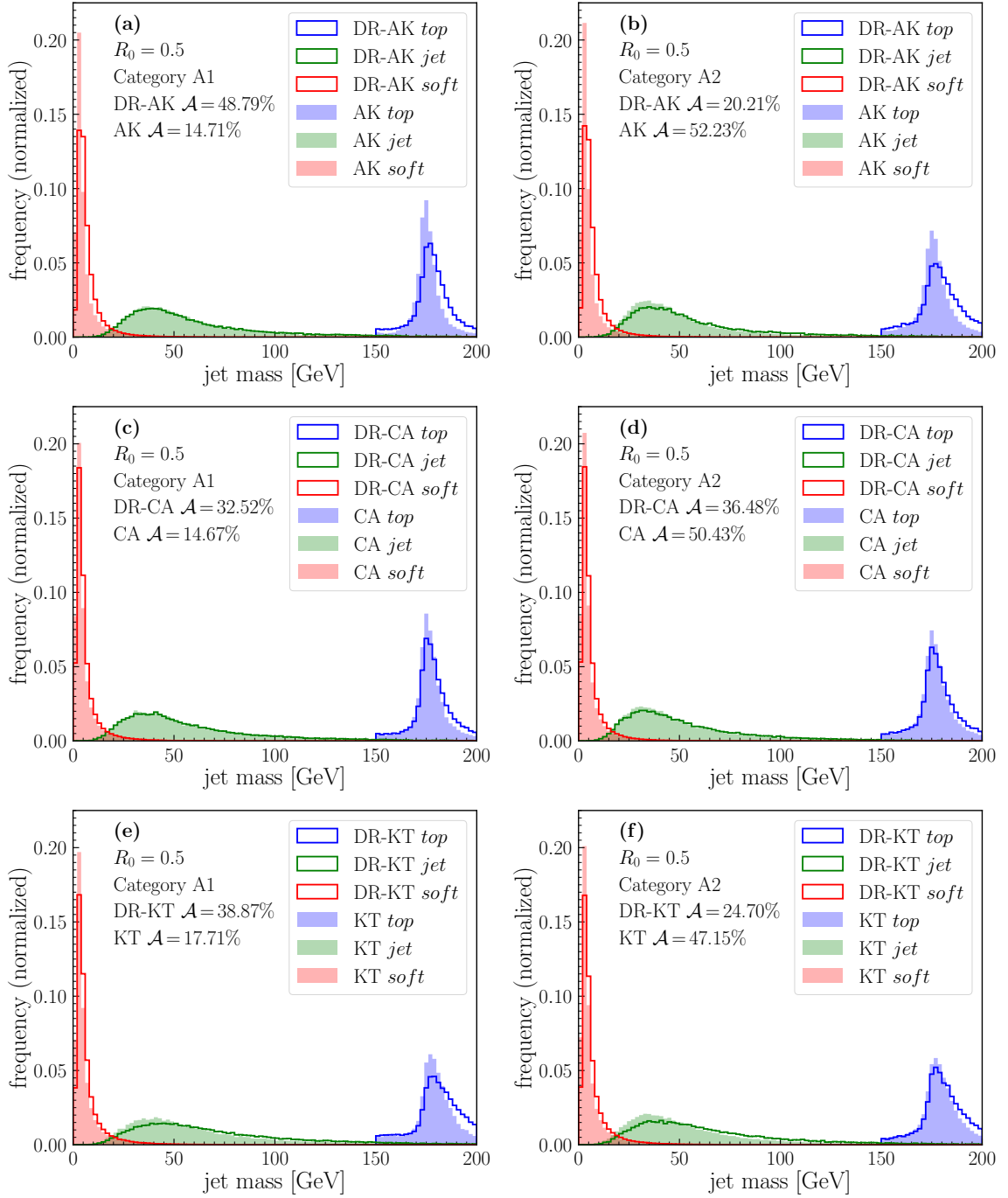


Figure 4: Normalized distribution of jet mass for the process $pp \rightarrow tj$. The left panel shows the distribution for category A1 events while the right panel is the distribution for category A2 events. The blue, green, and red histograms are for reconstructed top , hard jet , and $soft$ jets (defined in the text), respectively. The histograms, from top to bottom, are for AK, CA, and KT algorithms. The filled histograms correspond to fixed radius algorithms and the unfilled ones correspond to their dynamic radius (DR) counterparts.

One of the primary obligations of choosing the appropriate size for jets according to requirements is to avoid the rise of jet mass even with soft but widely separated constituents inside a jet. We, therefore, choose to show the distribution of masses of reconstructed *top* jets, reconstructed energetic *jets* in Fig. 4. The jet energy ranges corresponding to the mass distributions shown can be approximately 500-2000 GeV, as seen in Fig. 3. The left panel of the figure represents the distribution for category A1 events while the right panel represents the distribution for category A2 events. The blue, green, and red histograms are for reconstructed *top*, hard *jet*, and *soft jets*, respectively. The histograms, from top to bottom, are for anti- k_t , C/A, and k_t algorithms. The filled histograms are for standard jet clustering algorithms and the unfilled ones are their dynamic radius counterparts. In the legends, the prefix ‘DR’ to AK, CA, or KT stands for dynamic radius. In all the panels, the starting radius parameter has been taken to be $R_0 = 0.5$. For standard k_t -type algorithms, the starting radius is the fixed constant radius parameter, *i.e.*, $R_d = R_0$. The values for \mathcal{A} for different algorithms and different categories are quoted inside each panel of Fig. 4. In all the panels, it is seen that the acceptance efficiencies for A1 category events in the cases with dynamic radius algorithms are higher than their fixed radius counterparts.

An interesting feature to notice is that the mass distribution for the energetic *jet* remains almost the same for both the standard and dynamic radius jet clustering algorithms. The similarity between these two are more prominent for AK and CA algorithms and less so for the KT algorithm. This is expected as the KT algorithm starts to merge softer momenta first and then capture the harder ones almost at the end. As a result, this algorithm lets the size of the dynamic radius grow in the beginning and hence allows the softer hadron, even if they are a little wider, to merge with the evolving jet. The *top* jet mass distribution is also a little off with respect to their fixed radius analogue. These are not very problematic since jet grooming [77–83], trimming [84], or pruning [85, 86] methods help in cleaning soft and wide-angle radiation. A similar strategy of grooming is useful in the removal of *soft jets* as well.

The change in mass distribution for *top* jet but not for the energetic *jet* can easily be understood from the behaviour of the final radius $R_d = (R_0 + \sigma)$ [Eq. (2.5)] a jet has acquired. We, therefore, show the distribution of the final radii of the three different types of jets in Fig. 5. The three plots in the top panel are for category A1 events while those in the bottom panel are for category A2 events. For category A2 events, ‘*top c1*’ and ‘*top c2*’ labels represent the two constituent jets of reconstructed *top*. The distributions are shown for DR-AK, DR-CA, and DR-KT algorithms in Figs. 5(a,d), 5(b,e), and 5(c,f), respectively, with $R_0 = 0.5$ in each.

From all the histograms in Fig. 5, some clear features emerge. For the case of category A1 *top* jets, the final radius R_d grows to more than 0.6 with a peak at $R_d \simeq 0.75$, (approximately 50% increase with respect to the starting radius). On the other hand, for the energetic jets, R_d does not grow by much. This indicates that the radius grows dynamically according to the distribution of constituents inside the jet. The growth of the *soft jets* is higher compared to the hard *jets* candidates. In general, this will not be a problem in the heavy object finding since they can easily be eliminated by choosing an appropriate p_T or mass cuts. The story for the category A2 events is similar for *jets* and *soft jets*. The only

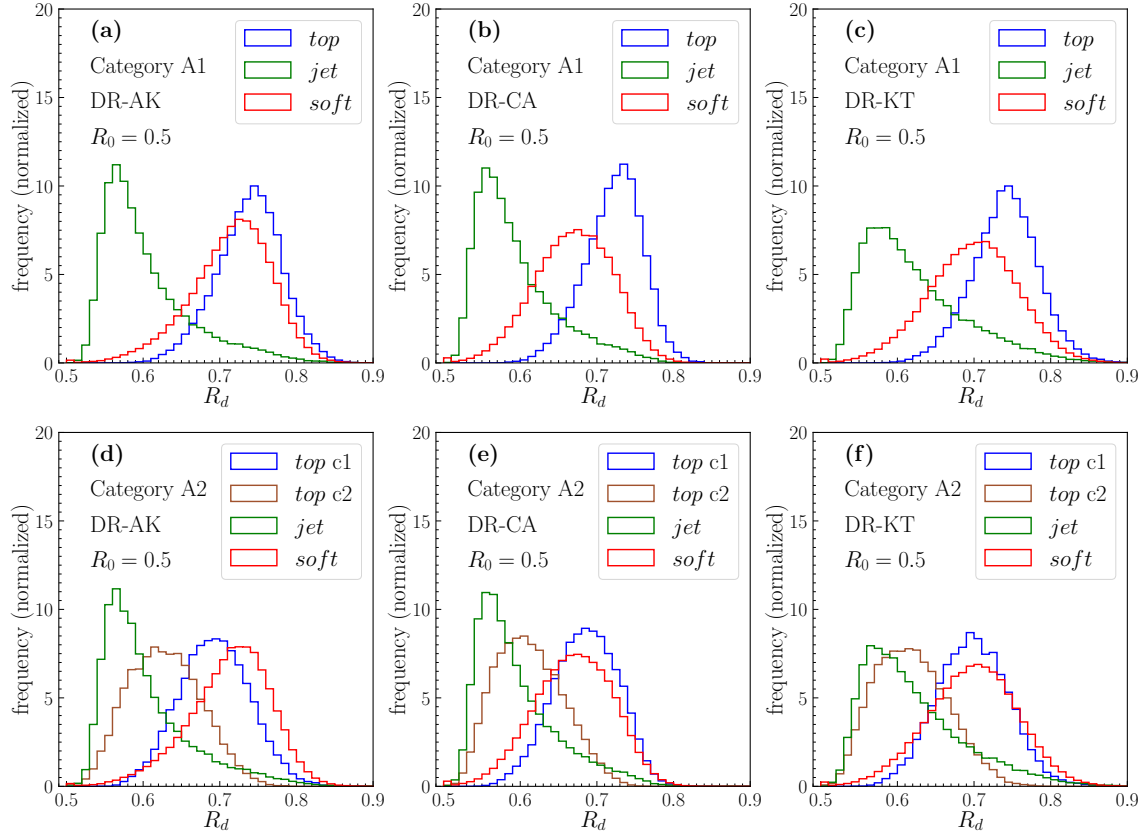


Figure 5: Normalized distribution of the final radius R_d of three different types of jets. The three plots in the top panel are for category A1 events while those in the bottom panel are for category A2 events. The conventions for the colours and labels ‘*top*’, ‘*jet*’, and ‘*soft*’ are the same as in Fig. 4. For category A2, ‘*topc1*’ and ‘*topc2*’ labels represent the two constituent jets of reconstructed *top*. The distributions are shown for DR-AK, DR-CA, and DR-KT algorithms in the panels (a,d), (b,e), and (e,f), respectively, with $R_0 = 0.5$.

difference is that the whole *top* could not be reconstructed as a single jet in these events. The normalized distributions of the final radii of these two constituent jets of reconstructed *tops* are plotted. These constituents tend to grow more than the energetic *jets*.

The values of acceptance efficiencies \mathcal{A} [Eq. (3.1)] for different category events vary with the choice of the value for the starting radius R_0 . If the starting radius is small, the algorithms fail to capture the fat jet. On the other hand, the large starting radius R_0 will capture the unwanted contamination coming from underlying events or radiations from other nearby showers. As a result, the jets will be unnecessarily fat and massive. There is a suitable range for R_0 within which the algorithms work better. We, therefore, show the variation of acceptance efficiencies \mathcal{A} as a function of starting radius R_0 in Fig. 6 for both categories A1 (blue) and A2 (red). The variations are shown for (DR-) AK, CA, and KT algorithms in panels (a), (b), and (c), respectively. As expected, for small R_0 values, the efficiencies for category A1 (blue lines) are negligible in both dynamic radius and fixed

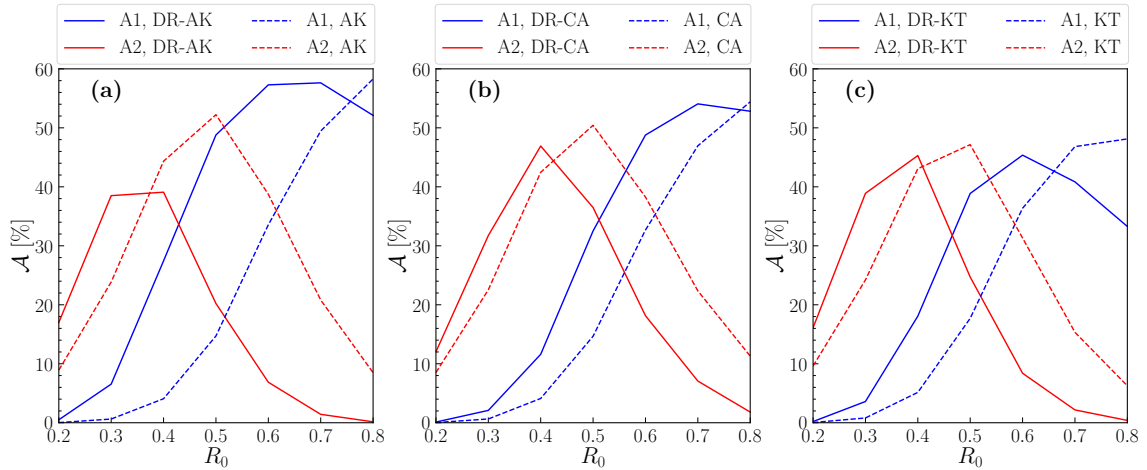


Figure 6: The variation of acceptance efficiency \mathcal{A} [Eq. (3.1)] as a function of starting radius R_0 for $pp \rightarrow tj$ SM process. The blue and red lines represent the variations of \mathcal{A} for categories A1 and A2 events, respectively. The dashed lines are for (a) AK, (b) CA, and (c) KT algorithm and the solid lines are for their dynamic radius versions.

radius analyses since the constituents of the entire *top* jet could not be captured with these small values of R_0 . Rather, the category A2 (red lines) which form the *top* with the help of two jets yields more \mathcal{A} . This picture changes once we tend towards higher values for $R_0 \simeq 0.5$ as more and more *top* jets are being reconstructed in the A1 category. As a result, the values of \mathcal{A} for the A2 category get reduced. In all the panels of Fig. 6, it is interesting to note that the dynamic radius algorithms (solid) yield higher values for \mathcal{A} than their fixed radius counterparts (dashed). This is indicative of the usefulness of the dynamic radius algorithm over the fixed radius ones. The dip in the blue solid lines after near $R_0 = 0.7$ is not essentially the failure of the algorithm. Rather, it is because of the capture of unwanted contaminations along with the radiation coming from the top. Therefore, the jet mass goes beyond 200 GeV, at which point we stop labelling them as a reconstructed *top* jet. Furthermore, a rough comparison among the curves in the three panels of Fig. 6 indicates that DR-AK is better suited than DR-CA and DR-KT algorithms.

3.2 Illustration II: $pp \rightarrow Vj$ Subprocess

A similar study has been performed in SM $pp \rightarrow Vj$, ($V = W$ or Z) processes. In order to ensure the formation of fat jets, a lower cut of 500 GeV on the p_T of the jet has been imposed at the time of generation of parton-level events via MG5. These events were then passed on to Pythia8 with *Monash 2013 Tune* [76] tune for parton showering and hadronization. The final state hadrons of these events were then sent to FastJet3 for jet clustering with starting radius $R_0 = 0.4$.

As before, we label the energetic jets coming from a jet clustering algorithm, as reconstructed ‘V’ or reconstructed ‘jet’ with the help of MG5 parton-level information. The rest

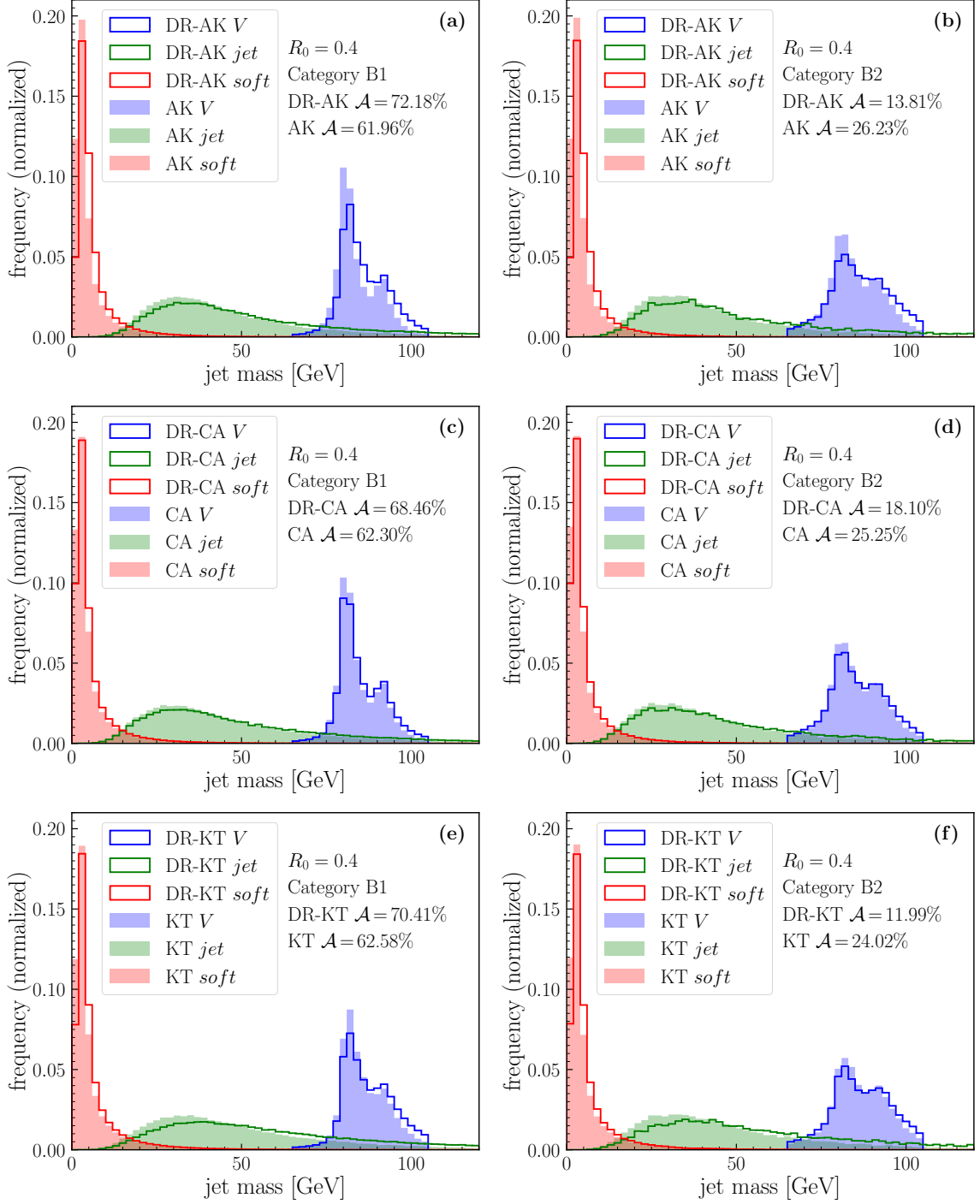


Figure 7: Normalized distributions of jet mass for the process $pp \rightarrow Vj$. The left panel shows jet mass distributions of category B1 events and the right panel is the distribution for category B2 events. The blue, green, and red histograms are for reconstructed V , energetic jet and $soft jets$ (defined in the text), respectively. The histograms, from top to bottom, are for AK, CA, and KT algorithms, respectively. The filled histograms correspond to fixed radius algorithms and the unfilled ones correspond to their dynamic radius (DR) analogues.

of the jets having $p_T > 5$ GeV are tagged as ‘*soft jets*’. As in the previous illustration, we classify the events into two separate categories based on the following criteria.

B1. An event was labelled as a category B1 event if it satisfies the following two conditions.

- A jet should have mass in the range (65, 105) GeV and $\Delta R(V^{\text{MG5}}, \text{jet}) < 0.5$. This jet was identified as a reconstructed V jet and we label them as ‘ V (B1)’ in further discussions.
- After the tagging of the V jet, another jet should have $p_T > 300$ GeV and $\Delta R(j^{\text{MG5}}, \text{jet}) < 0.5$. These jets are labelled as ‘*jet* (B1)’ in further discussions.

B2. An event, after failing to satisfy the criteria for the category B1, could be classified as a category B2 event subject to satisfying the below conditions.

- Two separate jets within 1.0 distance from the original vector boson (W or Z) and should have an invariant mass between 65 and 105 GeV. These two jets are tagged as constituent jets of the reconstructed ‘ V ’ jet. The final reconstructed ‘ V ’ jet should be within 0.5 distance from the original boson. This combination is labelled as ‘ V (B2)’.
- Another jet having $p_T > 300$ GeV and within 0.5 radii of the original jet and this is labelled as ‘*jet* (B2)’.

We show the jet mass distribution in Fig. 7 for SM $pp \rightarrow Vj$ process. All the distributions in the left panel of the figure represent the category B1 events and the distributions in the right panel are for category B2. The blue, green, and red histograms are for reconstructed ‘ V ’, *jet* and *soft jets*, respectively. The histograms, from top to bottom, are for AK, CA, and KT algorithms, respectively. The filled histograms are for standard jet clustering algorithms and the unfilled ones are their dynamic radius analogues. Quite clearly, the two peaks in the blue histograms, in all the distributions, correspond to the mass peaks of W and Z bosons. The jet mass distribution of the energetic jets using dynamic radius algorithms remains similar to their fixed radius counterparts. The increment in the percentage of the acceptance efficiencies \mathcal{A} [Eq. (3.1)] of category B1 events is representative of the appropriateness of using the dynamic radius algorithms over the standard ones in these types of scenarios.

We next show in Fig. 8 the normalized distributions of the final radius for three different types of jets, *viz.* ‘ V ’ jets, energetic *jets*, and *soft jets*. As in the $pp \rightarrow tj$ process, the fat V jets acquires a larger radius than the energetic *jets* after the dynamical expansion of the jet size. Here, again, the *soft jets* acquire a higher radius compared to the energetic *jets*. These *soft jets* are not of much concern since they are rather soft and hence they can be removed easily from the analysis.

In Fig. 9, we show the variation of \mathcal{A} [Eq. (3.1)] as a function of starting radius R_0 . In all the panels of the figure, the blue and red lines correspond to the variations for categories B1 and B2 events, respectively. The dashed lines are for fixed radius algorithms and the solid lines are for dynamic radius jet algorithms. The variations are shown for (a) AK, (b)

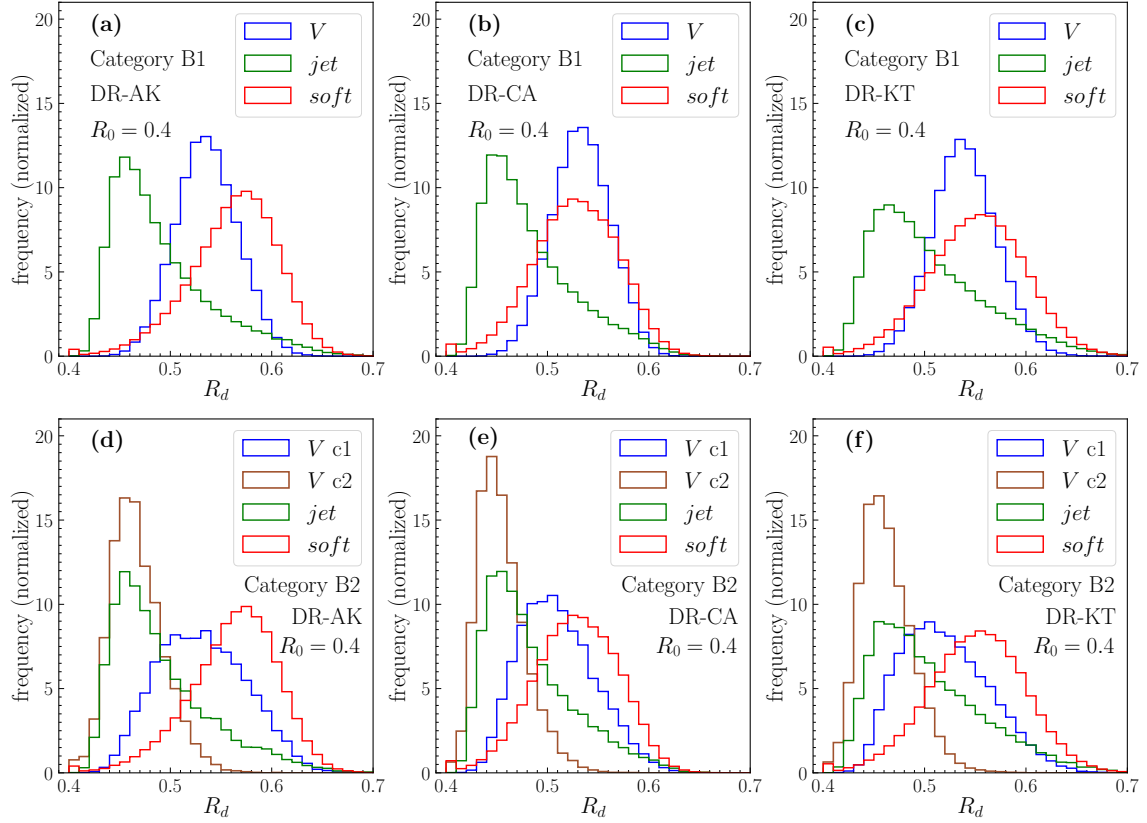


Figure 8: Normalized distribution of final radius R_d for the three different types of jets. The top panel represents the distributions of R_d in the category B1 events and the whole bottom panel is for category B2 events. The conventions for the colours and labels V , jet , and $soft$ are the same as Fig. 7. For category B2 events, ‘ V c1’ and ‘ V c2’ labels represent the two constituent jets of the reconstructed vector bosons. The distributions are shown for DR-AK, DR-CA, and DR-KT algorithms in the panels (a,d), (b,e), and (c,f), respectively, with $R_0 = 0.4$.

CA, and (c) KT algorithms. A quick observation of the curves tells us that the behaviour of these curves is similar to that of the curves in Fig. 6 except the monotonic decreasing nature of the category B2 curves. The reason is as follows: in the case of V jets, the jets are ‘two-pronged’ in nature. Therefore, the small radius jets can capture one of the two prongs of V jets, and thereby these two jets are able to reconstruct V jets in B2 category. However, as the starting radius R_0 is increasing, more and more events are migrating to category B1. The declining nature of the curves for large radii after 0.5 is because of the fact that the jets capture more hadrons than are required for their optimal size. As a result, the mass of the V jets tends to go beyond the mass window set to label them as V jets. Again, more variables than just the jet mass can help one to improve the tagger and hence the acceptance efficiency.

We conclude this section with the note that the dynamic radius jet algorithms are

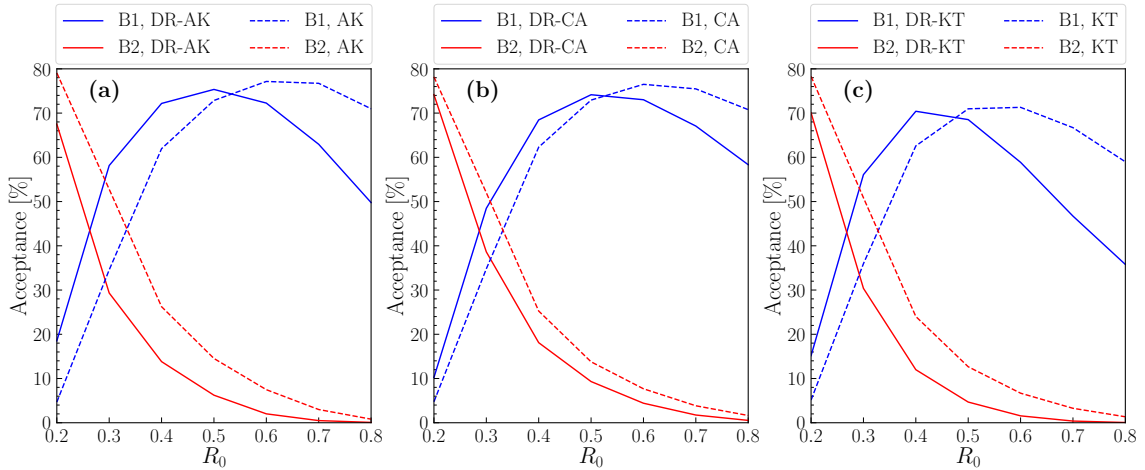


Figure 9: The variation of \mathcal{A} [Eq. (3.1)] as a function of the starting radius R_0 for $pp \rightarrow Vj$ SM process. The blue and red lines represent the values of \mathcal{A} for categories B1 and B2 events, respectively. The dashed lines are for (a) AK, (b) CA, and (c) KT algorithms. The solid lines are for their dynamic radius versions.

useful in finding fat as well as narrow jet in a single event in the colliders. We have successfully illustrated this in two SM processes, *viz.* $pp \rightarrow tj$ and $pp \rightarrow Vj$, at the 13 TeV LHC. A comparison among the three dynamic radius analogues of the standard k_t -type algorithm reveals that the DR-AK algorithm performs better compared to the DR-CA or the DR-KT algorithms.

4 Usefulness in BSM signals

We now illustrate the usefulness of the dynamic radius jet algorithm in the context of a scenario beyond the standard model (BSM). This is a scenario where an additional vectorlike singlet quark b' of charge $-1/3$ exists along with (d, s, b) . Such quarks occur, for example, in $E(6)$ grand unified theories, as also in some seesaw models of quark masses [87–92]. The b' can mix with the three SM down-type quarks when electroweak symmetry breaking takes place². This causes the mass eigenstate dominated by b' to decay into a top quark and a W boson. In addition, the mixing between a $T_3 = -1/2$ quark and one with $T_3 = 0$ induces flavour-changing Z - and Higgs-couplings in the b - b' sector. Thus the b' , produced via strong interactions at the LHC, has the decays $b' \rightarrow tW$, $b' \rightarrow bZ$, $b' \rightarrow bh$. The detailed theoretical framework and the resulting phenomenology have been discussed widely in the literature [59, 93–101].

The currently available data from the LHC restrict $m_{b'}$ to be no less than 1.3–1.5 TeV [102–105]. When such a massive quark decays thereafter, its decay products are consider-

²In the following discussion, we shall (a) denote this mass eigenstate itself by b' , (b) assume that ordinary-exotic quark mixing takes place involving only the third family sequential quark, namely, b , and (c) parametrize the b - b' mixing by the angle θ .

ably lighter compared to it. Therefore the b' decay products are considerably boosted, so as to produce fat jets. Furthermore, the difference in mass between two product particles leads to jets of varying degrees of fatness.

Since our purpose here is to show the efficacy of the dynamic radius jet algorithm, we illustrate our main points in the context of $pp \rightarrow b'\bar{b}'$ followed by each b' decaying into a top quark and a W boson. The t 's and the W 's thus give rise to energetic jets of different radii. We demonstrate below how our newly developed algorithm can capture the identity of the ensuing final state. While the present work is aimed at capturing the essence of our proposed jet algorithm, a more detailed discussion, including combinations of all the three aforementioned decay channels of the b' , is going to be presented in a separate work [106].

$m_{b'}$	$\sin \theta_L$	$\sin \theta_R$
1.3 TeV	0.12	8.02×10^{-3}

Table 1: Values of some important parameters of the vectorlike singlet b' model considered for the illustration.

The model has been implemented in a Mathematica-based package **SARAH** [107–109]. The Universal FeynRules Output (UFO) [110] generated by SARAH is then used in MG5 for the generation of parton-level events. The parameter card for MG5 has been generated using spectrum generator **SPheno** [111, 112]. The values for the important parameters of the model are tabulated in Table 1. The angles θ_L and θ_R in the table represent the mixing angle between SM b quark and exotic b' quark of chirality left and right, respectively. After the generation of the MG5 parton-level events, the rest of the analysis pipeline is the same as the previous illustrations of SM processes.

In this illustration, we choose DR-AK, based on the discussion in the previous section. We show the resultant jets having $p_T > 30$ GeV formed out of the hadrons generated by Pythia8 in Fig. 10. The left panel shows the positions of the generated hadrons and jets constructed using the AK algorithm with $R_0 = 0.5$. The right panel shows the same for the DR-AK algorithm. In both panels, the red dots represent the position of final state hadrons in the η - ϕ plane and the size of each dot is proportional to the $\sqrt{p_T}$ of the hadron. The unfilled circles represent the final radius (R_d) of a jet. The teal dots represent the constituents of boosted fat ‘W’ jets. The green, blue, and purple (wherever applicable) dots represent the constituents of the fat ‘top’ jet. The yellow dots containing texts represent the position of the MG5 parton-level p_T -hard quarks after the decay of top or W . The mothers of the q or b are mentioned in the subscripts of q or b .

An interesting point to observe in Fig. 10(b) is that the DR-AK yields only 4 jets, which are representative of 2 fat W and 2 fat t jets. However, in Fig. 10, the fixed radius algorithm could form the fat W jets but fails to capture the entirety of the two fat t jets. One, of course, can use a bigger radius in the AK algorithm to capture the whole of the top jet. However, this will make the W jet unnecessarily fat. This demonstrates the utility of the dynamic radius jet algorithm.

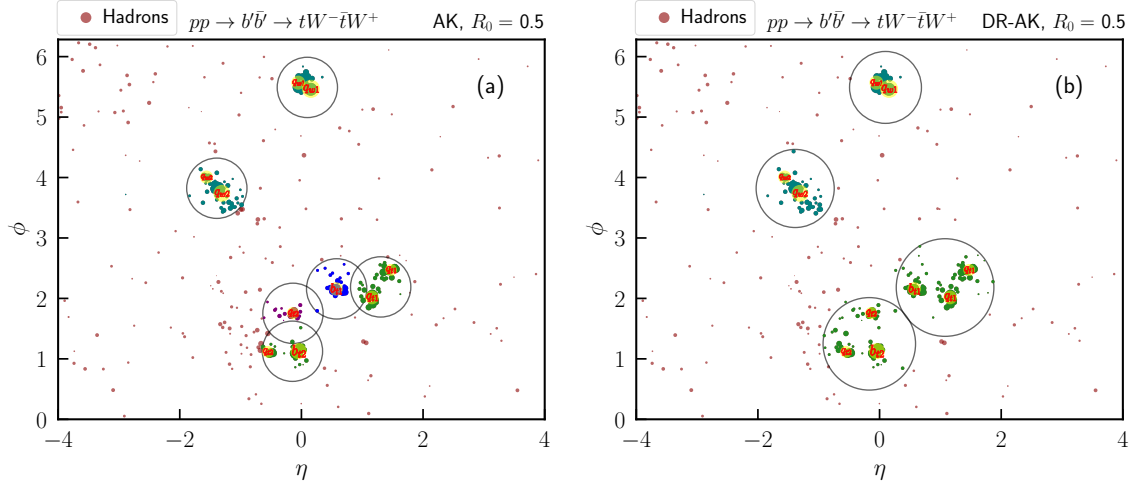


Figure 10: The distribution of final state hadrons and jets in η - ϕ plane for an example event. The colours and sizes of the dots and circles follow the same convention as Fig. 1. The teal coloured dots represent the constituents of hard fat ‘W’ jets. The green and blue (wherever applicable) dots represent the constituents of the fat ‘top’ jet. The yellow dots containing texts represent the position of the hard quarks after the decay of top or W which are mentioned as the subscripts of q or b . The plots are shown for (a) AK and (b) DR-AK algorithms.

To study the goodness of DR-AK quantitatively, we define the following criteria for tagging of top and W jets.

- A jet having mass in the range (150, 200) GeV and having $\Delta R(\text{top}^{\text{truth}}, \text{jet}) < 0.5$ is identified as a reconstructed top jet.
- A jet will be called W jet if it has a mass in the range (65, 105) GeV and is within 0.5 distance from the original MG5 parton-level W boson.

Similar to the illustrations with SM processes, we classify the events into different categories. Due to the complex nature of the final states, we have classified the events into more than two categories in the present scenario. The realization is based on the following understanding.

- Out of the two W ’s coming directly from b' in an event, the number of reconstructed W as fat jet from the algorithm could be 0, 1, or 2. We call these reconstructed fat W jets as primary W jets.
- Similarly, out of the two t quarks, the number of reconstructed t as fat jets can be 0, 1, or 2.
- In some particular cases, the whole top may not be reconstructed, but the W boson coming from the top quarks may be reconstructed. These are referred to as secondary W jets in the subsequent discussions.

Based on the above observations, we classify the events into different categories, whose generic name is given as Cij , where i and j are two integers encoding the number of reconstructed top and reconstructed W 's, respectively. For the present scenario, the allowed value for i does not exceed two. For a given i , the values for j should not exceed $4 - i$. That is, to say, $i \leq 2$ and $j \leq 4 - i$. An exhaustive list of all possible categories is tabulated in Table 2. For example, the event shown in Fig. 10 would be categorized as C22 for the DR-AK algorithm while the same event would be classified as C03 for the AK algorithm. One may again subdivide some of the categories into subcategories based on how many W jets are coming directly from b' (primary W) and how many of them are coming from the decay of the top quark (secondary W). Therefore, the generic name for the subcategories can be given as $Cijk$ with i , j , and k being the numbers of reconstructed top , primary W , and secondary W jets. The possible ranges for i , j , and k are $0 \leq i, j \leq 2$ and $0 \leq k \leq 2 - i$.

Category	Subcategory	No. of top jet	No. of primary W jet	No. of secondary W jet
C22	C220	2	2	0
C21	C210	2	1	0
C20	C200	2	0	0
C13	C121	1	2	1
C12	C120	1	2	0
	C111	1	1	1
C11	C110	1	1	0
	C101	1	0	1
C10	C100	1	0	0
C04	C022	0	2	2
C03	C021	0	2	1
	C012	0	1	2
C02	C020	0	2	0
	C011	0	1	1
	C002	0	0	2
C01	C010	0	1	0
	C001	0	0	1
C00	C000	0	0	0

Table 2: The definitions of the list of categories and subcategories as according to how many fat jets can be reconstructed from the jet algorithm.

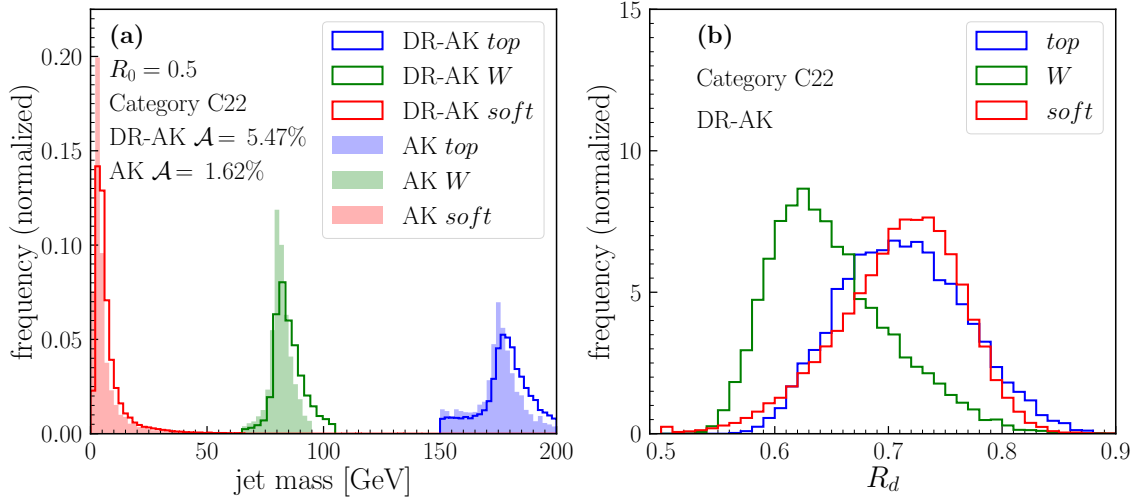


Figure 11: (a) The normalized distribution of jet mass of the category C22 events for the $pp \rightarrow b'\bar{b}' \rightarrow tW^- \bar{t}W^+$ process. The blue, green, and red histograms are reconstructed top , W , and $soft$ jets, respectively. The unfilled histograms are for the jets clustered using the DR-AK algorithm while the filled ones are for the jets using the AK clustering algorithm. (b) The normalized distribution of the final radii of top , W , and $soft$ jets with blue, green, and red colours, respectively. For both panels, $R_0 = 0.5$ was used and any additional jets having $p_T > 5$ GeV were considered as a $soft$ jet.

We plot the normalized distribution of jet mass of the category C22 events in Fig. 11(a). Jets were clustered using $R_0 = 0.5$. In the plot, the blue, green, and red histograms are reconstructed top , W , and $soft$ jets, respectively. The unfilled histograms are for the jets clustered using the DR-AK algorithm, and the filled ones are for the jets using the AK clustering algorithm. Any untagged jet with $p_T > 5$ GeV was considered to be a $soft$ jet. Fig. 11(b) shows the normalized distribution for the finally acquired radii of different jets for category C22 events. The desirable feature of the reconstructed W jets being narrower than the reconstructed top jets is clearly apparent in the figure. Here, again, the $soft$ jets are growing to larger radius are expected. However, as discussed in the previous section, they can be removed from an analysis by p_T or jet mass cuts.

The values of \mathcal{A} [Eq. (3.1)] for the two different algorithms, *viz.* DR-AK and AK are also quoted in Fig. 11(a). These values (1.62% for AK and 5.47% for DR-AK), clearly, indicate that the dynamic radius jet algorithm is working better while probing the correct mass windows for the particles. The shift of the mass distribution towards larger values is indicative of capturing little extra than required. As discussed previously, this can be rectified by the techniques of grooming [77–81], trimming [84], or pruning [85, 86]. Furthermore, going beyond just the jet mass to tag the top or W jets would further help in extracting signals.

The variation of \mathcal{A} as a function of initial radius R_0 is shown in Fig. 12 for six categories, namely C22, C21, C20, C13, C12, and C11. These categories have at least one top jet identified within 0.5 distance from the MG5 parton-level top quark. The solid blue lines

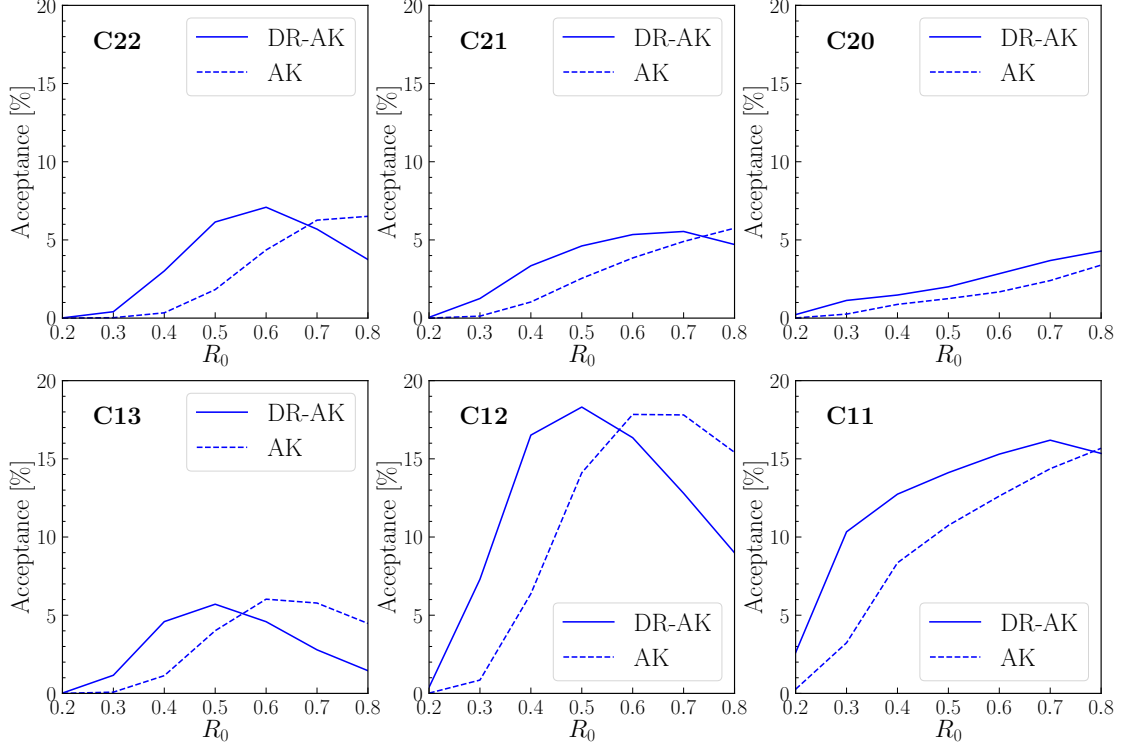


Figure 12: The variation of \mathcal{A} [Eq. (3.1)] as a function of initial radius R_0 for six categories, namely C22, C21, C20, C13, C12, and C11. The solid blue lines are for the DR-AK algorithm, and the dashed lines are for the AK algorithm. The jets are clustered with $R_0 = 0.5$.

represent the efficiencies for the DR-AK algorithm, and the dashed lines are representative of the AK algorithm. For the case of dynamic radius, the quintessential feature is the initial increment in the acceptance efficiencies \mathcal{A} up to $R_0 = 0.5$, and, beyond this value, the efficiencies decrease. The reason for this is an unnecessary accumulation of hadrons and making the jets bigger than their optimal size. However, for the AK algorithm, the efficiencies keep on increasing until $R_0 = 0.7$, which is kind of the optimal radius for this scenario. The most important point to note is that up to $R_0 = 0.5$, the efficiencies for the DR-AK algorithm are higher than those for the AK algorithm. This feature, again, establishes the utility of using dynamic radius algorithms over fixed radius ones.

In the end, we look at the bar plot of the acceptance efficiencies \mathcal{A} for all the categories in Fig. 13. The blue and green bars are for DR-AK and AK algorithms, respectively. The initial radius R_0 is taken to be 0.5. The numbers under the curly braces below the x -axis represent the values of \mathcal{A} for the categories which capture 2 *tops*, 1 *top*, 0 *top*, and none of the *top* or *W* jets. The important observation in this regard is that the categories containing 2 *top* and 1 *top* jets have better efficiencies for the dynamic radius algorithm than the fixed radius one. This means that the events, where the AK algorithm could not capture the whole of the *top* constituents, the DR-AK algorithm could capture the full *tops*. Thus the credence of our proposed algorithm is established in a BSM context as well.

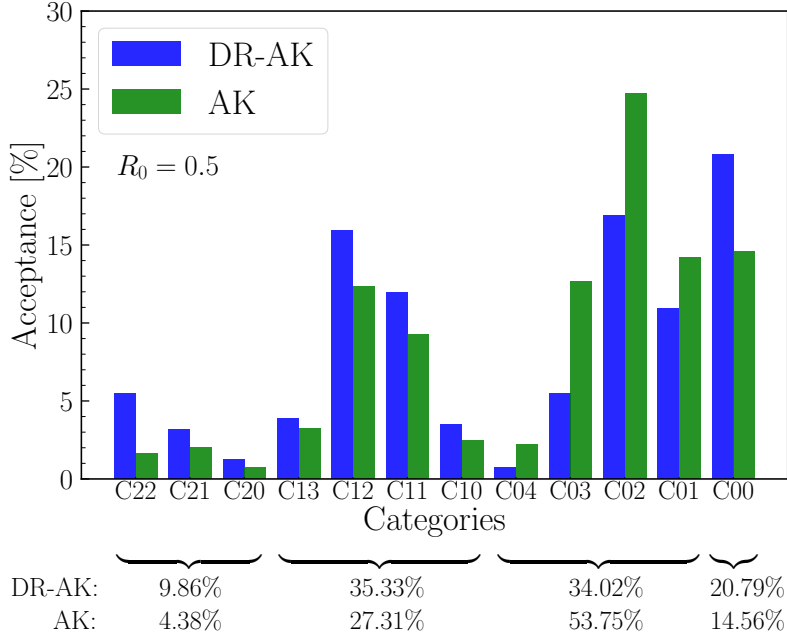


Figure 13: Bar plot of \mathcal{A} for different categories for jet algorithms with $R_0 = 0.5$. The blue, and green bars are for DR-AK and AK algorithm respectively. From left to right, The numbers under the braces represent the values of \mathcal{A} for the categories which capture 2 *top*, 1 *top*, 0 *top*, and none of the *top* or *W* jets.

5 Summary and Outlook

We go beyond the most popular jet clustering algorithms, where the formation of jets is performed using a fixed radius parameter. These algorithms return fixed-sized jets corresponding to the input radius parameter. In this work, an attempt is made to make the radius of each jet variable depending on the kinematics and hadronic activity in the neighbourhood of an evolving jet. The proposed method is based on the standard k_t -type sequential recombination jet clustering algorithms with the incorporation of the dynamic nature of the radius parameter.

Starting from a reasonable radius parameter, during the process of formation of a jet, the radius of each evolving jet is allowed to grow based on *fuzziness* inside it. For this work, the measure of the fuzziness of each evolving jet is chosen to be the ‘ p_T -weighted’ standard deviation of the inter-particle distances (in the η - ϕ plane) of the particles inside the evolving jet.

After describing the proposed method, we have presented two different SM processes, *viz.* $pp \rightarrow tj$ and $pp \rightarrow Wj + Zj$, to demonstrate some applicabilities of the dynamic radius jet clustering algorithm. In these two processes, differently-sized jets are expected in a single event. In the two SM process examples, we observe that the jets are being formed with radii varying in size on a jet-by-jet basis. In terms of the acceptance efficiency [Eq. (3.1)], we show that the performance of the dynamic radius algorithm is better compared to their

fixed radius counterparts. We take up a scenario beyond the Standard Model for further illustration, where a vectorlike $SU(2)_L$ singlet charge $-1/3$ quark b' is added. We study jet clustering in $pp \rightarrow b'\bar{b}'$ followed by each b' decaying into tW . Once more, our proposed method turns out to be effective in the reconstruction of the final state particles.

In the examples given above, the dynamicity has been incorporated in the radius parameter of the standard k_t -type sequential recombination algorithm. The central idea is the usage of *fuzziness* of an evolving jet to appropriately increase its radius starting from a starting radius R_0 . Although examples with only one measure of *fuzziness* have been shown in this work, one may consider other appropriate measures, depending upon the underlying physics process or the final goal of the analysis. Therefore, the idea of the dynamic radius jet algorithm should not be restricted only to this particular measure. The applicability of these possibilities will be presented in a separate work. In a nutshell, the idea of dynamic radius jet clustering algorithm on a jet-by-jet basis is useful in collider studies and will be beneficial in searches driven by processes in SM as well as BSM.

Acknowledgments

The authors thank Jayita Lahiri for useful discussions during the initial phase of the work.

References

- [1] J.M. Campbell, J.W. Huston and W.J. Stirling, *Hard Interactions of Quarks and Gluons: A Primer for LHC Physics*, *Rept. Prog. Phys.* **70** (2007) 89 [[hep-ph/0611148](#)].
- [2] R.K. Ellis, W.J. Stirling and B.R. Webber, *QCD and collider physics*, vol. 8, Cambridge University Press (2, 2011), [10.1017/CBO9780511628788](#).
- [3] G.F. Sterman and S. Weinberg, *Jets from Quantum Chromodynamics*, *Phys. Rev. Lett.* **39** (1977) 1436.
- [4] J.E. Huth et al., *Toward a standardization of jet definitions*, in *1990 DPF Summer Study on High-energy Physics: Research Directions for the Decade (Snowmass 90)*, pp. 0134–136, 12, 1990.
- [5] G.C. Blazey et al., *Run II jet physics*, in *Physics at Run II: QCD and Weak Boson Physics Workshop: Final General Meeting*, pp. 47–77, 5, 2000 [[hep-ex/0005012](#)].
- [6] S.D. Ellis, J. Huston, K. Hatakeyama, P. Loch and M. Tonnesmann, *Jets in hadron-hadron collisions*, *Prog. Part. Nucl. Phys.* **60** (2008) 484 [[0712.2447](#)].
- [7] G.P. Salam, *Towards Jetography*, *Eur. Phys. J. C* **67** (2010) 637 [[0906.1833](#)].
- [8] S. Catani, Y.L. Dokshitzer, M. Olsson, G. Turnock and B.R. Webber, *New clustering algorithm for multi - jet cross-sections in e^+e^- annihilation*, *Phys. Lett. B* **269** (1991) 432.
- [9] S. Catani, Y.L. Dokshitzer, M.H. Seymour and B.R. Webber, *Longitudinally invariant K_t clustering algorithms for hadron hadron collisions*, *Nucl. Phys. B* **406** (1993) 187.
- [10] S.D. Ellis and D.E. Soper, *Successive combination jet algorithm for hadron collisions*, *Phys. Rev. D* **48** (1993) 3160 [[hep-ph/9305266](#)].
- [11] Y.L. Dokshitzer, G.D. Leder, S. Moretti and B.R. Webber, *Better jet clustering algorithms*, *JHEP* **08** (1997) 001 [[hep-ph/9707323](#)].

- [12] M. Wobisch and T. Wengler, *Hadronization corrections to jet cross-sections in deep inelastic scattering*, in *Workshop on Monte Carlo Generators for HERA Physics (Plenary Starting Meeting)*, pp. 270–279, 4, 1998 [[hep-ph/9907280](#)].
- [13] M. Cacciari, G.P. Salam and G. Soyez, *The anti- k_t jet clustering algorithm*, *JHEP* **04** (2008) 063 [[0802.1189](#)].
- [14] A.J. Larkoski, J. Thaler and W.J. Waalewijn, *Gaining (Mutual) Information about Quark/Gluon Discrimination*, *JHEP* **11** (2014) 129 [[1408.3122](#)].
- [15] P. Gras, S. Höche, D. Kar, A. Larkoski, L. Lönnblad, S. Plätzer et al., *Systematics of quark/gluon tagging*, *JHEP* **07** (2017) 091 [[1704.03878](#)].
- [16] J. Gallicchio and M.D. Schwartz, *Quark and Gluon Tagging at the LHC*, *Phys. Rev. Lett.* **107** (2011) 172001 [[1106.3076](#)].
- [17] J. Gallicchio and M.D. Schwartz, *Quark and Gluon Jet Substructure*, *JHEP* **04** (2013) 090 [[1211.7038](#)].
- [18] J.R. Andersen et al., *Les Houches 2015: Physics at TeV Colliders Standard Model Working Group Report*, in *9th Les Houches Workshop on Physics at TeV Colliders*, 5, 2016 [[1605.04692](#)].
- [19] B. Bhattacharjee, S. Mukhopadhyay, M.M. Nojiri, Y. Sakaki and B.R. Webber, *Quark-gluon discrimination in the search for gluino pair production at the LHC*, *JHEP* **01** (2017) 044 [[1609.08781](#)].
- [20] P.T. Komiske, E.M. Metodiev and J. Thaler, *An operational definition of quark and gluon jets*, *JHEP* **11** (2018) 059 [[1809.01140](#)].
- [21] S. Bright-Thonney and B. Nachman, *Investigating the Topology Dependence of Quark and Gluon Jets*, *JHEP* **03** (2019) 098 [[1810.05653](#)].
- [22] A.J. Larkoski and E.M. Metodiev, *A Theory of Quark vs. Gluon Discrimination*, *JHEP* **10** (2019) 014 [[1906.01639](#)].
- [23] A.K. Nayak, S.K. Rai and T. Samui, *Improving Heavy Dijet Resonance Searches Using Jet Substructure at the LHC*, *Eur. Phys. J. C* **81** (2021) 130 [[1912.03511](#)].
- [24] D. Reichelt, S. Caletti, O. Fedkevych, S. Marzani, S. Schumann and G. Soyez, *Phenomenology of jet angularities at the LHC*, *JHEP* **03** (2022) 131 [[2112.09545](#)].
- [25] I.W. Stewart and X. Yao, *Pure quark and gluon observables in collinear drop*, *JHEP* **09** (2022) 120 [[2203.14980](#)].
- [26] S. Bright-Thonney, I. Moutl, B. Nachman and S. Prestel, *Systematic quark/gluon identification with ratios of likelihoods*, *JHEP* **12** (2022) 021 [[2207.12411](#)].
- [27] S.D. Ellis, A. Hornig, T.S. Roy, D. Krohn and M.D. Schwartz, *Qjets: A Non-Deterministic Approach to Tree-Based Jet Substructure*, *Phys. Rev. Lett.* **108** (2012) 182003 [[1201.1914](#)].
- [28] S.D. Ellis, A. Hornig, D. Krohn and T.S. Roy, *On Statistical Aspects of Qjets*, *JHEP* **01** (2015) 022 [[1409.6785](#)].
- [29] *Les Houches 2017: Physics at TeV Colliders Standard Model Working Group Report*, 3, 2018.
- [30] S. Marzani, G. Soyez and M. Spannowsky, *Looking inside jets: an introduction to jet substructure and boosted-object phenomenology*, vol. 958, Springer (2019), [10.1007/978-3-030-15709-8](#), [[1901.10342](#)].

- [31] A.J. Larkoski, G.P. Salam and J. Thaler, *Energy Correlation Functions for Jet Substructure*, *JHEP* **06** (2013) 108 [[1305.0007](#)].
- [32] A.J. Larkoski, I. Moult and D. Neill, *Analytic Boosted Boson Discrimination*, *JHEP* **05** (2016) 117 [[1507.03018](#)].
- [33] A.J. Larkoski, I. Moult and D. Neill, *Power Counting to Better Jet Observables*, *JHEP* **12** (2014) 009 [[1409.6298](#)].
- [34] A.J. Larkoski, I. Moult and D. Neill, *Building a Better Boosted Top Tagger*, *Phys. Rev. D* **91** (2015) 034035 [[1411.0665](#)].
- [35] D. Adams et al., *Towards an Understanding of the Correlations in Jet Substructure*, *Eur. Phys. J. C* **75** (2015) 409 [[1504.00679](#)].
- [36] I. Moult, L. Necib and J. Thaler, *New Angles on Energy Correlation Functions*, *JHEP* **12** (2016) 153 [[1609.07483](#)].
- [37] R.S. Chivukula, K.A. Mohan, D. Sengupta and E.H. Simmons, *Characterizing boosted dijet resonances with energy correlation functions*, *JHEP* **03** (2018) 133 [[1710.04661](#)].
- [38] J. Thaler and K. Van Tilburg, *Identifying Boosted Objects with N -subjettiness*, *JHEP* **03** (2011) 015 [[1011.2268](#)].
- [39] I.W. Stewart, F.J. Tackmann, J. Thaler, C.K. Vermilion and T.F. Wilkason, *X_{Cone} : N -jettiness as an Exclusive Cone Jet Algorithm*, *JHEP* **11** (2015) 072 [[1508.01516](#)].
- [40] A. Dey and T. Samui, *Jet Substructure and Multivariate Analysis Aid in Polarization Study of Boosted, Hadronic W Fatjet at the LHC*, [2110.02773](#).
- [41] J. Thaler and K. Van Tilburg, *Maximizing Boosted Top Identification by Minimizing N -subjettiness*, *JHEP* **02** (2012) 093 [[1108.2701](#)].
- [42] Z. Han, *Tracking the Identities of Boosted Particles*, *Phys. Rev. D* **86** (2012) 014026 [[1112.3378](#)].
- [43] T. Plehn and M. Spannowsky, *Top Tagging*, *J. Phys. G* **39** (2012) 083001 [[1112.4441](#)].
- [44] G. Kasieczka, T. Plehn, T. Schell, T. Strebler and G.P. Salam, *Resonance Searches with an Updated Top Tagger*, *JHEP* **06** (2015) 203 [[1503.05921](#)].
- [45] M. Dasgupta, L. Schunk and G. Soyez, *Jet shapes for boosted jet two-prong decays from first-principles*, *JHEP* **04** (2016) 166 [[1512.00516](#)].
- [46] G.P. Salam, L. Schunk and G. Soyez, *Dichroic subjettiness ratios to distinguish colour flows in boosted boson tagging*, *JHEP* **03** (2017) 022 [[1612.03917](#)].
- [47] Z. Han, M. Son and B. Tweedie, *Top-Tagging at the Energy Frontier*, *Phys. Rev. D* **97** (2018) 036023 [[1707.06741](#)].
- [48] J.A. Aguilar-Saavedra, J.H. Collins and R.K. Mishra, *A generic anti-QCD jet tagger*, *JHEP* **11** (2017) 163 [[1709.01087](#)].
- [49] A. Das, P. Konar and A. Thalapillil, *Jet substructure shedding light on heavy Majorana neutrinos at the LHC*, *JHEP* **02** (2018) 083 [[1709.09712](#)].
- [50] L. Moore, K. Nordström, S. Varma and M. Fairbairn, *Reports of My Demise Are Greatly Exaggerated: N -subjettiness Taggers Take On Jet Images*, *SciPost Phys.* **7** (2019) 036 [[1807.04769](#)].

- [51] D. Napoletano and G. Soyez, *Computing N -subjettiness for boosted jets*, *JHEP* **12** (2018) 031 [[1809.04602](#)].
- [52] K. Agashe, J.H. Collins, P. Du, S. Hong, D. Kim and R.K. Mishra, *Detecting a Boosted Diboson Resonance*, *JHEP* **11** (2018) 027 [[1809.07334](#)].
- [53] L. Bradshaw, R.K. Mishra, A. Mitridate and B. Ostdiek, *Mass Agnostic Jet Taggers*, *SciPost Phys.* **8** (2020) 011 [[1908.08959](#)].
- [54] J.A. Aguilar-Saavedra and B. Zaldívar, *Jet tagging made easy*, *Eur. Phys. J. C* **80** (2020) 530 [[2002.12320](#)].
- [55] Y. Mehtar-Tani, A. Soto-Ontoso and K. Tywoniuk, *Tagging boosted hadronic objects with dynamical grooming*, *Phys. Rev. D* **102** (2020) 114013 [[2005.07584](#)].
- [56] A. Bhardwaj, J. Dutta, P. Konar, B. Mukhopadhyaya and S.K. Rai, *Boosted jet techniques for a supersymmetric scenario with gravitino LSP*, *JHEP* **10** (2020) 083 [[2007.00351](#)].
- [57] S. De, V. Rentala and W. Shepherd, *Measuring the polarization of boosted, hadronic W bosons with jet substructure observables*, [2008.04318](#).
- [58] S. Bhattacharya, M. Guchait and A.H. Vijay, *Boosted top quark tagging and polarization measurement using machine learning*, *Phys. Rev. D* **105** (2022) 042005 [[2010.11778](#)].
- [59] D. Choudhury, K. Deka and N. Kumar, *Looking for a vectorlike B quark at the LHC using jet substructure*, *Phys. Rev. D* **104** (2021) 035004 [[2103.10655](#)].
- [60] M. Dasgupta and J. Helliwell, *Investigating top tagging with Y_m -Splitter and N -subjettiness*, *JHEP* **10** (2021) 092 [[2108.09317](#)].
- [61] Y. Lu, A. Romero, M.J. Fenton, D. Whiteson and P. Baldi, *Resolving extreme jet substructure*, *JHEP* **08** (2022) 046 [[2202.00723](#)].
- [62] A. Bhardwaj, K. Bhide, T. Mandal, S. Mitra and C. Neeraj, *Discovery prospects of a vectorlike top partner decaying to a singlet boson*, *Phys. Rev. D* **106** (2022) 075024 [[2204.09005](#)].
- [63] A. Dey, R. Rahaman and S.K. Rai, *Fatjet signatures of heavy neutrinos and heavy leptons in a left-right model with universal seesaw at the HL-LHC*, [2207.06857](#).
- [64] B. Bhattacharjee, C. Bose, A. Chakraborty and R. Sengupta, *Boosted top tagging and its interpretation using Shapley values*, [2212.11606](#).
- [65] P.K. Das, P. Konar, S. Kundu and S. Show, *Jet substructure probe to unfold singlet-doublet dark matter in the presence of non-standard cosmology*, [2301.02514](#).
- [66] CMS collaboration, *Measurement of jet substructure observables in $t\bar{t}$ events from proton-proton collisions at $\sqrt{s} = 13\text{TeV}$* , *Phys. Rev. D* **98** (2018) 092014 [[1808.07340](#)].
- [67] ATLAS collaboration, *Measurement of jet-substructure observables in top quark, W boson and light jet production in proton-proton collisions at $\sqrt{s} = 13\text{ TeV}$ with the ATLAS detector*, *JHEP* **08** (2019) 033 [[1903.02942](#)].
- [68] CMS collaboration, *Study of quark and gluon jet substructure in Z +jet and dijet events from pp collisions*, *JHEP* **01** (2022) 188 [[2109.03340](#)].
- [69] D. Krohn, J. Thaler and L.-T. Wang, *Jets with Variable R* , *JHEP* **06** (2009) 059 [[0903.0392](#)].

- [70] L. Mackey, B. Nachman, A. Schwartzman and C. Stansbury, *Fuzzy Jets*, *JHEP* **06** (2016) 010 [[1509.02216](#)].
- [71] M. Cacciari, G.P. Salam and G. Soyez, *FastJet User Manual*, *Eur. Phys. J. C* **72** (2012) 1896 [[1111.6097](#)].
- [72] M. Cacciari and G.P. Salam, *Dispelling the N^3 myth for the k_t jet-finder*, *Phys. Lett. B* **641** (2006) 57 [[hep-ph/0512210](#)].
- [73] J. Alwall, R. Frederix, S. Frixione, V. Hirschi, F. Maltoni, O. Mattelaer et al., *The automated computation of tree-level and next-to-leading order differential cross sections, and their matching to parton shower simulations*, *JHEP* **07** (2014) 079 [[1405.0301](#)].
- [74] T. Sjöstrand, S. Mrenna and P.Z. Skands, *PYTHIA 6.4 Physics and Manual*, *JHEP* **05** (2006) 026 [[hep-ph/0603175](#)].
- [75] T. Sjöstrand, S. Ask, J.R. Christiansen, R. Corke, N. Desai, P. Ilten et al., *An introduction to PYTHIA 8.2*, *Comput. Phys. Commun.* **191** (2015) 159 [[1410.3012](#)].
- [76] P. Skands, S. Carrazza and J. Rojo, *Tuning PYTHIA 8.1: the Monash 2013 Tune*, *Eur. Phys. J. C* **74** (2014) 3024 [[1404.5630](#)].
- [77] J.M. Butterworth, A.R. Davison, M. Rubin and G.P. Salam, *Jet substructure as a new Higgs search channel at the LHC*, *Phys. Rev. Lett.* **100** (2008) 242001 [[0802.2470](#)].
- [78] M. Dasgupta, A. Fregoso, S. Marzani and G.P. Salam, *Towards an understanding of jet substructure*, *JHEP* **09** (2013) 029 [[1307.0007](#)].
- [79] A.J. Larkoski, S. Marzani, G. Soyez and J. Thaler, *Soft Drop*, *JHEP* **05** (2014) 146 [[1402.2657](#)].
- [80] S. Marzani, L. Schunk and G. Soyez, *A study of jet mass distributions with grooming*, *JHEP* **07** (2017) 132 [[1704.02210](#)].
- [81] S. Marzani, L. Schunk and G. Soyez, *The jet mass distribution after Soft Drop*, *Eur. Phys. J. C* **78** (2018) 96 [[1712.05105](#)].
- [82] F.A. Dreyer, L. Necib, G. Soyez and J. Thaler, *Recursive Soft Drop*, *JHEP* **06** (2018) 093 [[1804.03657](#)].
- [83] Y. Mehtar-Tani, A. Soto-Ontoso and K. Tywoniuk, *Dynamical grooming of QCD jets*, *Phys. Rev. D* **101** (2020) 034004 [[1911.00375](#)].
- [84] D. Krohn, J. Thaler and L.-T. Wang, *Jet Trimming*, *JHEP* **02** (2010) 084 [[0912.1342](#)].
- [85] S.D. Ellis, C.K. Vermilion and J.R. Walsh, *Techniques for improved heavy particle searches with jet substructure*, *Phys. Rev. D* **80** (2009) 051501 [[0903.5081](#)].
- [86] S.D. Ellis, C.K. Vermilion and J.R. Walsh, *Recombination Algorithms and Jet Substructure: Pruning as a Tool for Heavy Particle Searches*, *Phys. Rev. D* **81** (2010) 094023 [[0912.0033](#)].
- [87] V.D. Barger, N. Deshpande, R.J.N. Phillips and K. Whisnant, *Extra Fermions in E_6 Superstring Theories*, *Phys. Rev. D* **33** (1986) 1912.
- [88] T.G. Rizzo, *Phenomenology of Exotic Particles in $E(6)$ Theories*, *Phys. Rev. D* **34** (1986) 1438.
- [89] B. Mukhopadhyaya and S. Nandi, *Evading the top mass bound at the Tevatron: New signals for the top*, *Phys. Rev. Lett.* **66** (1991) 285.

- [90] B. Mukhopadhyaya and S. Nandi, *Collider implications of singlet fermions*, *Phys. Rev. D* **46** (1992) 5098.
- [91] R.S. Chivukula, B.A. Dobrescu, H. Georgi and C.T. Hill, *Top Quark Seesaw Theory of Electroweak Symmetry Breaking*, *Phys. Rev. D* **59** (1999) 075003 [[hep-ph/9809470](#)].
- [92] M. Gillioz, R. Gröber, A. Kapuvari and M. Mühlleitner, *Vector-like Bottom Quarks in Composite Higgs Models*, *JHEP* **03** (2014) 037 [[1311.4453](#)].
- [93] J. Maalampi and M. Roos, *Flavor Mixing in the Presence of a Fourth Down Quark*, *Phys. Lett. B* **188** (1987) 487.
- [94] A. Raychaudhuri, *Is the b Quark Mixed with a Vector Like Quark*, *Phys. Rev. D* **40** (1989) 833.
- [95] V.D. Barger, M.S. Berger and R.J.N. Phillips, *Quark singlets: Implications and constraints*, *Phys. Rev. D* **52** (1995) 1663 [[hep-ph/9503204](#)].
- [96] T.C. Andre and J.L. Rosner, *Exotic $Q = -1/3$ quark signatures at high-energy hadron colliders*, *Phys. Rev. D* **69** (2004) 035009 [[hep-ph/0309254](#)].
- [97] S. Gopalakrishna, T. Mandal, S. Mitra and R. Tibrewala, *LHC Signatures of a Vector-like b'* , *Phys. Rev. D* **84** (2011) 055001 [[1107.4306](#)].
- [98] J.A. Aguilar-Saavedra, R. Benbrik, S. Heinemeyer and M. Pérez-Victoria, *Handbook of vectorlike quarks: Mixing and single production*, *Phys. Rev. D* **88** (2013) 094010 [[1306.0572](#)].
- [99] A. Girdhar, B. Mukhopadhyaya and M. Patra, *Distinguishing Signatures of top-and bottom-type heavy vectorlike quarks at the LHC*, *Phys. Rev. D* **91** (2015) 055015 [[1404.3374](#)].
- [100] S.A.R. Ellis, R.M. Godbole, S. Gopalakrishna and J.D. Wells, *Survey of vector-like fermion extensions of the Standard Model and their phenomenological implications*, *JHEP* **09** (2014) 130 [[1404.4398](#)].
- [101] K. Das, T. Li, S. Nandi and S.K. Rai, *New signals for vector-like down-type quark in $U(1)$ of E_6* , *Eur. Phys. J. C* **78** (2018) 35 [[1708.00328](#)].
- [102] CMS collaboration, *A search for bottom-type, vector-like quark pair production in a fully hadronic final state in proton-proton collisions at $\sqrt{s} = 13$ TeV*, *Phys. Rev. D* **102** (2020) 112004 [[2008.09835](#)].
- [103] CMS collaboration, *Search for pair production of vector-like quarks in leptonic final states in proton-proton collisions at $\sqrt{s} = 13$ TeV*, [2209.07327](#).
- [104] ATLAS collaboration, *Search for pair-production of vector-like quarks in pp collision events at $\sqrt{s} = 13$ TeV with at least one leptonically decaying Z boson and a third-generation quark with the ATLAS detector*, [2210.15413](#).
- [105] ATLAS collaboration, *Search for pair-produced vector-like top and bottom partners in events with large missing transverse momentum in pp collisions with the ATLAS detector*, [2212.05263](#).
- [106] B. Mukhopadhyaya, T. Samui and R.K. Singh, *in preparation*.
- [107] F. Staub, *SARAH*, [0806.0538](#).
- [108] F. Staub, *SARAH 4 : A tool for (not only SUSY) model builders*, *Comput. Phys. Commun.* **185** (2014) 1773 [[1309.7223](#)].

- [109] F. Staub, *Exploring new models in all detail with SARAH*, *Adv. High Energy Phys.* **2015** (2015) 840780 [[1503.04200](#)].
- [110] C. Degrande, C. Duhr, B. Fuks, D. Grellscheid, O. Mattelaer and T. Reiter, *UFO - The Universal FeynRules Output*, *Comput. Phys. Commun.* **183** (2012) 1201 [[1108.2040](#)].
- [111] W. Porod, *SPheno, a program for calculating supersymmetric spectra, SUSY particle decays and SUSY particle production at e^+e^- colliders*, *Comput. Phys. Commun.* **153** (2003) 275 [[hep-ph/0301101](#)].
- [112] W. Porod and F. Staub, *SPheno 3.1: Extensions including flavour, CP-phases and models beyond the MSSM*, *Comput. Phys. Commun.* **183** (2012) 2458 [[1104.1573](#)].